Journal of Constructional Steel Research 204 (2023) 107870

Contents lists available at ScienceDirect

Journal of Constructional Steel Research

journal homepage: www.elsevier.com/locate/jcsr

Cyclic friction-slip behaviour of G350-steel bolted connections

Andrew William Lacey, Wensu Chen *, Hong Hao *

Centre for Infrastructural Monitoring and Protection, School of Civil and Mechanical Engineering, Curtin University, Australia

ARTICLE INFO

Keywords:
Cyclic test
Steel joint
Slip factor
Surface treatment
Paint coating
Prefab
Modular building
Inter-module connection

ABSTRACT

In this study, an experimental program was performed to investigate the cyclic friction-slip behaviour of AS/NZS 3678–350 (G350) steel with different surface finishes. Fifteen bolted steel connections consisting of EN 1090–2 slip factor test assemblies with M16 bolts were prepared and tested with five commonly used surface finishes including inorganic zinc silicate (IZS), epoxy zinc primer (EZP), aliphatic acrylic polyurethane (PUR), abrasive blasted (SA2), and clean mill scale (CMS). The first initial force-slip stiffness and the first slip factor are reported for each surface finish and compared with the existing literature and design standards. An empirical model is proposed to predict the initial slip behaviour based on the first slip factor and initial stiffness, and its accuracy is demonstrated for the coated and uncoated steel. The effects of the cyclic load are then considered, and the cyclic slip factor and initial stiffness are evaluated and discussed. Finally, corresponding empirical models are proposed for the cyclic slip factor and friction-slip stiffness as a function of the cumulative displacement.

1. Introduction

Predictable and consistent, stable sliding between the interfaces of structural steel connections is desirable. If the slip resistance is less than the design value, i.e., understrength, then the connection could slip prematurely. The slip displacements could cause local damage, or, in modular steel structures, for example, they could accumulate over the height of the building leading to global failures [1]. Alternatively, the cyclic slipping could lead to pounding in the joint and may result in a reduction of the fatigue strength as it is subjected to tension-compression cycles [2]. Conversely, the connection sliding may be relied upon to limit the loads transferred or to dissipate energy [3], in which case overstrength of the slip resistance could lead to an unsafe design.

The authors previously summarised the numerous existing studies on the slip factor of typical structural steel materials [4]. The data for Australian steel materials, however, was lacking, hence, the short term friction-slip behaviour of AS/NZS 3678–350 [5] steel was investigated following the method of EN 1090–2 [6] Annex G in this study. For the clean mill scale (CMS) surfaces the 95% confidence interval for the mean slip factor was 0.3146 ± 0.0154 ($\pm 4.91\%$, $N = 9$). The CMS layer was smooth and separated the steel substrates reducing the adhesion, i.e., inter-atomic attraction between the steel surfaces, resulting in a relatively low slip factor. However, as the friction resistance was exceeded and the surfaces began sliding, the CMS layer could be damaged revealing the underlying steel and, hence, increasing the slip factor. Consequently, some force-slip behaviours exhibited several small slips prior to a major slip, although the effect varied among the specimens depending on the composition and thickness of the CMS layer. Due to this dependence of the slip factor on the accumulated surface damage and, hence, loading history, further study of the slip factor due to cyclic loading was suggested.

The slip factors for the sand blasted surfaces were 0.5516 ± 0.0311 ($\pm 5.65\%$, $N = 5$) and 0.5525 ± 0.0348 ($\pm 6.31\%$, $N = 5$) for the Sa 1 and Sa 3 surface finishes [7], respectively. Hence, with the degree of sand blasting defined by visual assessment according to ISO 8501-1 [8], the slip factor was reported to be insensitive to the surface finish. Compared with the CMS specimens, the sand blasted specimens had a more severe friction-slip behaviour (i.e., higher initial force-slip stiffness with a sudden increase in slip as the friction resistance was exceeded) which was attributed to mechanical interlock of the rougher surfaces. After testing, the faying surfaces around the bolts were smooth and shiny suggesting that the sliding had flattened and smoothed the surfaces. Again, the slip factor depended on the accumulated surface damage and further study of the slip factor due to cyclic loading was indicated.

Despite the need, relatively few studies have considered the cyclic friction-slip behaviour of bolted steel connections with a standard arrangement suitable for the evaluation of the slip factor development. In 1978 Vitelleschi et al. [9] published a study on the influence of cyclic loading on the slip factor for slip resistant bolted connections with

* Corresponding authors.
E-mail addresses: wensu.chen@curtin.edu.au (W. Chen), hong.hao@curtin.edu.au (H. Hao).

https://doi.org/10.1016/j.jcsr.2023.107870
Received 4 December 2022; Received in revised form 14 February 2023; Accepted 17 February 2023
Available online 3 March 2023

Table 1
List of 15 specimens and associated parameters.

Specimen	Faying surface reference	Steel surface preparation [7]	Coating system	Dry film thickness (μm)		
				Low	High	Average
SP1–3	**IZS**	Abrasive Blast (Sa 2.5, Very thorough)	*1st Coat:* 75 μm **inorganic zinc silicate** (Zinc Clad 6001, Grey, Flat)	66	120	87
SP4–6	**EZP**	Sa 2.5	*1st Coat:* 75 μm **epoxy zinc primer** (Intergard 251, Buff, Matt)	60	96	78
SP7–9	**PUR**	Sa 2.5	*1st Coat:* 75 μm epoxy zinc primer (Intergard 251) *2nd Coat:* 75 μm aliphatic acrylic **polyurethane** (Interthane 990, Light Grey, High Gloss)	139	176	152
SP10–12	**SA2**	Abrasive Blast (**Sa 2**, Thorough)	–	–	–	–
SP13–15	**CMS**	**Clean Mill Scale**	–	–	–	–

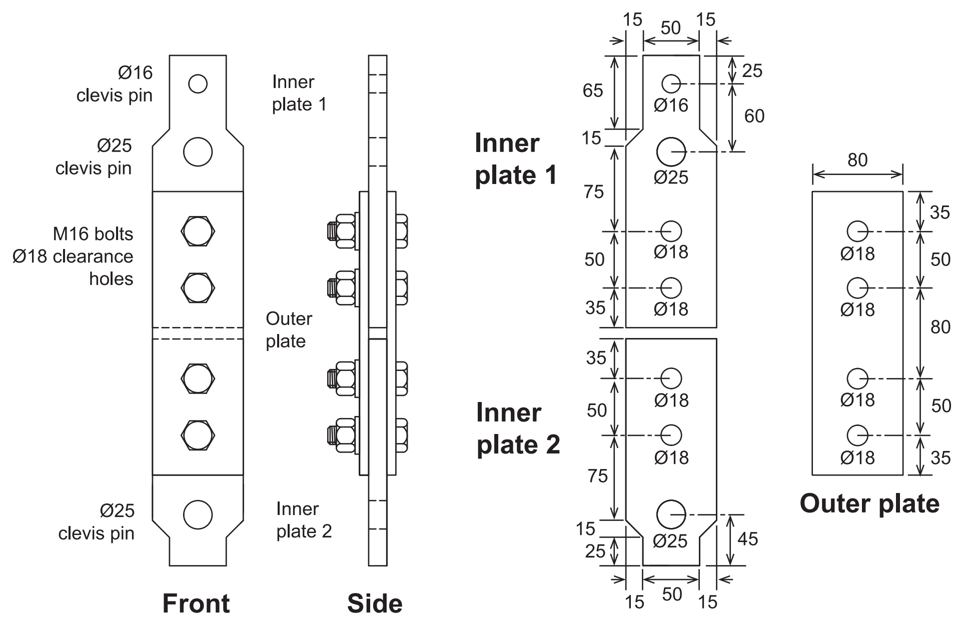

Fig. 1. Nominal specimen details. All dimensions are in millimetres (mm).

varying surface finishes including galvanized, clean mill scale (CMS), urethane chromate primer, and inorganic zinc silicate (IZS). The symmetrical double cover plated butt joint specimens were composed of 12.5 and 25 mm thick outer and inner plates, respectively, connected by two 19 mm diameter bolts with a tensile strength of 870 MPa installed in 21 mm clearance holes.

The specimens [9] were subjected to four or five cycles with load applied at 0.25 mm/min while the variation of the slip factor was recorded. For the galvanized specimens, the slip factor increased with each cycle, e.g., increasing from 0.20 to 0.35 over the cycles. This finding was supported by a prior study [2] where it was reported that the slip factor increased due to galling of the relatively soft and uneven zinc coating. For primed surfaces, however, the slip factor decreased, e.g., from 0.28 to 0.26 over four cycles [9]. For the IZS the slip occurred suddenly, such that a cyclic load could not be applied without damaging the transducers, and it was accompanied by a sudden drop in the load. For the CMS, the slip factor initially started to decrease, before increasing again after which the specimen finally slipped and the load dropped to zero. Generally, it was reported that if the applied cyclic load exceeds the slip resistance, then the slip factor will reduce with successive cycles for all the surfaces considered, except for galvanized. It was noted, however, that insufficient data was obtained to establish the behaviour of the IZS, while further study of the sudden slip and corresponding drop in load for the IZS and CMS specimens was recommended due to the potential for an unbuttoning effect in multi-bolted joints. It should be noted, however, that details of the substrate surface profile or the dry film thickness of the coating applied were lacking, limiting the practical application of the work.

Sliding along steel interfaces causes surface damage which generates wear particles. Sometimes the development of wear particles has a beneficial effect. If, for example, an interface is formed between two surfaces with a clean mill scale finish, a stable sliding behaviour can be achieved with minimal cumulative travel required, as the relatively soft mill scale fragments have a lubricating effect [10]. Still, the initial presence of the mill scale layer separates the underlying steel resulting in a low initial friction coefficient. As the mill scale layer is damaged, the underlying steel is exposed and the friction coefficient increases before the generated wear particles are sufficient to offer a lubricating effect. In contrast, uncoated mild steel to mild steel interfaces can exhibit severe stick-slip behaviours and load spiking due to the development of wear particles [10–12]. As the steel wear particles develop, they occupy space at the interface causing the plates to move outward, increasing the bolt load and, hence, the slip resistance. In interfaces consisting of two similar materials, e.g., mild steel interfaces, the wear particles are not easily absorbed into a softer layer, hence, the interface is particularly vulnerable to load spiking and seizure [11]. Still, the effect of the mill scale was not entirely clear and further study is required, especially for bolted connections with standard round holes rather than long slotted holes as adopted in the referenced work [10].

The need for the present work is justified, firstly, by the limited studies considering the Australian grade steel. Steel materials that conform to Australian specifications may have different chemical composition and mechanical property requirements compared to similar grades of steel that are manufactured to other standards. The variations

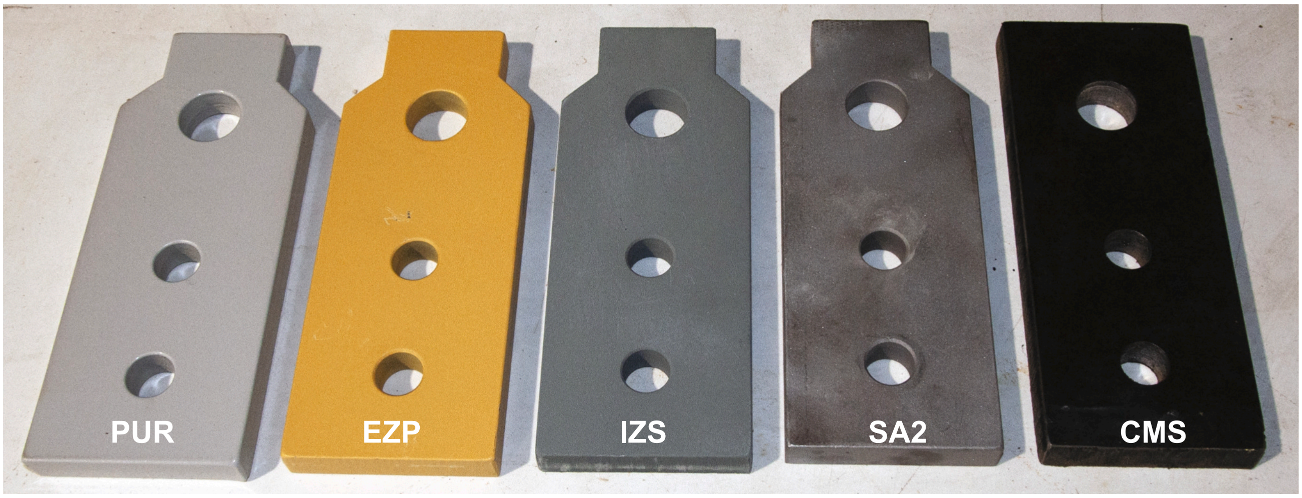

Fig. 2. Typical specimen surface preparations.

in mechanical properties can influence the slip factor by altering the amount of plastic deformation of the steel substrate [13]. Second, bolted steel connections are vulnerable to corrosion which is typically addressed by the addition of protective coatings, and paint is commonly adopted. Therefore, it is essential to investigate the effect of painted coatings on the shear behaviour of the AS/NZS 3678–350 (G350) bolted steel connections. Finally, in current practice, the friction-slip behaviour of bolted steel connections is characterised by the first slip factor and the first initial force-slip stiffness. However, even for the standard slip factor test specimens, cyclic loading can damage the faying surfaces thereby changing the subsequent friction-slip behaviour. To enable the development of more accurate models, it is essential to understand the effect of cyclic loading on the friction-slip behaviours of the common structural steel materials, such as G350 steel. Therefore, the present study aims to establish the effect of cyclic loading on the friction-slip behaviour of G350 bolted steel connections consisting of the standard EN 1090–2 [6] slip factor test assembly with M16 8.8/s bolts. The cyclic loading can lead to damage of the faying surfaces which can change the effective friction coefficient. Moreover, bolt preload can be affected by the cyclic loading, firstly through a general reduction in the preload through the load cycles, but also due to the surface damage which can produce wear particles that affect the bolt preload. Cyclic loads were applied and the slip resistance for each cycle was measured, hence, the cyclic slip factors were determined as a measure of both the change in friction coefficient and bolt preload.

2. Experimental program

2.1. Specimens

Fifteen specimens, named SP1–15, were prepared with varying surface preparation and coatings (Table 1). Each standard slip factor test specimen [6] consisted of two inner 16 mm thick, and two outer 8 mm thick AS/NZS 3678–350 steel plates which were connected via 4-M16 EN 14399–3 [14] k2 HR property class 8.8 bolts (Fig. 1). Inner plate 1 (Fig. 1) had nominal φ16 and φ25 mm clearance holes to suit the φ16 and φ25 upper clevis pins. Two pins were provided in this case to provide stability against out of plane rotation when the specimen was subjected to a compression force. Inner plate 2, however, had only one nominal φ25 clearance hole to suit the single φ25 lower clevis pin. 18 mm clearance holes were provided in all the plates to suit the M16 bolts.

Prior to testing, each specimen was reduced to its shortest length, such that each plate was firmly in contact with the bolt shanks (see also §3.1). In this way, when the initial tension force was applied, the initial resistance would be due only to the friction developed between the clamped plates. Moreover, the total upwards translation of inner plate 1 (Fig. 1) would be 4 mm, assuming both the upper and the lower joints slipped 2 mm due to the bolt hole tolerance, i.e., φ18 mm hole – φ16 mm bolt shank. The 2 mm bolt hole tolerance, however, was a nominal value. The actual average bolt hole tolerance was 2.3 mm and the sample standard deviation was 0.051 mm ($n = 15$), mainly due to variation in the bolt shank diameter. In practice the bolt shanks would not be consistently located; rather, the position of the bolt shank in the bolt hole would vary. Consequently, in practice, the maximum slip displacement before the bolt shanks come into bearing with the plates could be less than that in the experiments.

The M16 bolts were then tensioned using a torque wrench. A two-stage tightening process was adopted to give a bolt preload of 95 kN based on the manufacturer supplied k-value ($k_m = 0.126$, $V_k = 0.040$). The torque required to give the specified preload ($F_{p,C}$) was determined according to AS/NZS 1252.1 [15] as

$$M_r = k_m D F_{p,C} \tag{1}$$

where the nominal bolt diameter (D) was 16 mm, and the coefficient (k_m) was determined through bolt assembly tests according to Appendix D of AS/NZS 1252.1 [15] and EN 14399–2 [16]. From five assembly tests conducted by the bolt manufacturer, the average k-factor (k_m) was 0.126 and the coefficient of variation, i.e., ratio of the standard deviation to the mean, was 0.040. An indication of the uncertainty of the resulting bolt preload can be given by the 95% confidence interval for the mean preload which can be estimated as 95 kN ± 3.33 kN. As will be discussed in §3.2, this variation of the bolt preload affects, for example, the first slip factor obtained for the specimens.

Specimens SP13–15 had the surfaces maintained in a clean mill scale (CMS) condition (Fig. 2). In contrast, specimens SP10–12 had the surfaces abrasive blast cleaned to class Sa 2, i.e., thorough blast cleaning [7] (also known as *industrial* or *commercial blast cleaning* in the SPC/NACE joint standard). The blast cleaning class was verified by visually comparing the prepared steel surface with the representative photographs given in ISO 8501-1 [8]. The coated specimens (SP1–9) were similarly abrasive (garnet) blast cleaned to class Sa 2.5, i.e., very thorough blast cleaning [7] (also known as *near-white metal blast cleaning*). Additionally, the surface profile, i.e., peak-to-valley height, was assessed using profile replicating tape in accordance with AS 3894.5 [17]. That is, plastic tape was impressed into the substrate profile using a burnishing tool to produce a reverse replica which could be measured via a spring-loaded micrometer [17]. The measured surface profile ranged from 70 to 75 μm. The substrates were then coated by spraying in a controlled shop environment. Common paint coatings were selected following review of AS 2312.1 [18], namely inorganic zinc silicate (IZS),

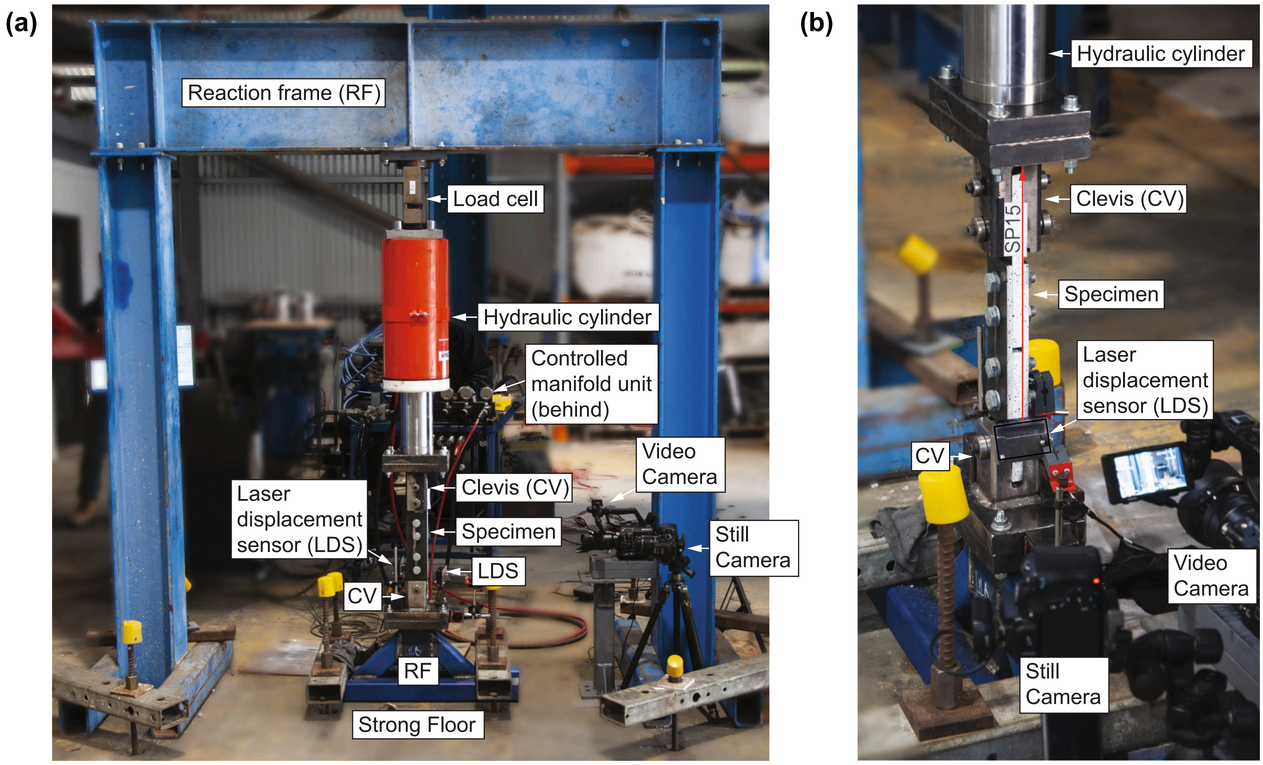

Fig. 3. (a) Overall test setup and (b) closer view of specimen front.

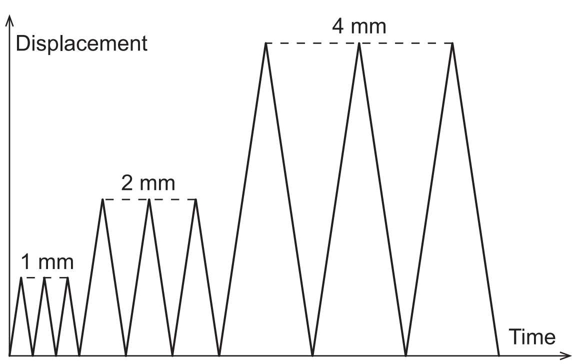

Fig. 4. Loading protocol.

epoxy zinc primer (EZP), and epoxy zinc primer + acrylic polyurethane (PUR) (Table 1). The dry film thicknesses were subsequently measured using a calibrated coating thickness gauge and the actual minimum, maximum and area averaged values were recorded (Table 1). In accordance with standard practice, the coatings were accepted if the actual dry film thickness was in the range of 80% to 120% of the specified nominal value (e.g., 60 to 90 μm for nominal 75 μm). The time allowed for coating curing was 54 days.

2.2. Test setup

Each specimen was installed between a lower and an upper clevis (Fig. 3). The lower clevis (CV) provided restraint against vertical translation via connection to the strong floor. The upper clevis connected the specimen to the hydraulic cylinder, which was controlled to provide the cyclic loading. The applied load was measured by a load cell. Two laser displacement sensors (LDS) measured the change in the vertical distance between the clevis end plates (Fig. 3b). The cyclic loading was applied based on the laser measurements. A speckled pattern was applied to one side of the specimen, and the movements of this surface were recorded by a video camera to allow post-test analysis of the relative movements between the specimen plates. A still camera recorded additional images at 4 s intervals.

2.3. Loading protocol

A force-controlled load with target displacements was applied. The pressure applied to the hydraulic cylinder was manually controlled via a manifold unit, thereby controlling the force applied to the specimen. The specimen displacement was monitored via two laser displacement sensors, and the pressure was changed slowly to achieve the target displacements. Three phases of incremental amplitudes were applied: 3 cycles each at 1 mm, 2 mm, and 4 mm (Fig. 4), i.e., 25%, 50% and 100% of the nominal maximum displacement. This loading protocol was supported by the related previous studies [10–12,19–21].

The hydraulic pressure was changed slowly and, generally, the resulting relative displacement rate was limited to 0.02 mm/s, allowing the quasi-static slip resistance to be obtained, although larger displacement rates were possible after the friction resistance was exceeded in each cycle. As the specimens were reduced to their shortest length prior to testing, the displacements were applied only in the positive direction, indicating extension of the specimen. A tension force was applied and increased until the target displacement was reached. Then, the loading direction was reversed, and a compression force was applied, pushing the specimen back to its original length. In this way, although only positive displacements were applied, the corresponding force cycled between positive and negative values, i.e., tension and compression.

3. Results and analysis

Images were extracted from the recorded videos at 1 s intervals, and digital image correlation was carried out to establish the vertical

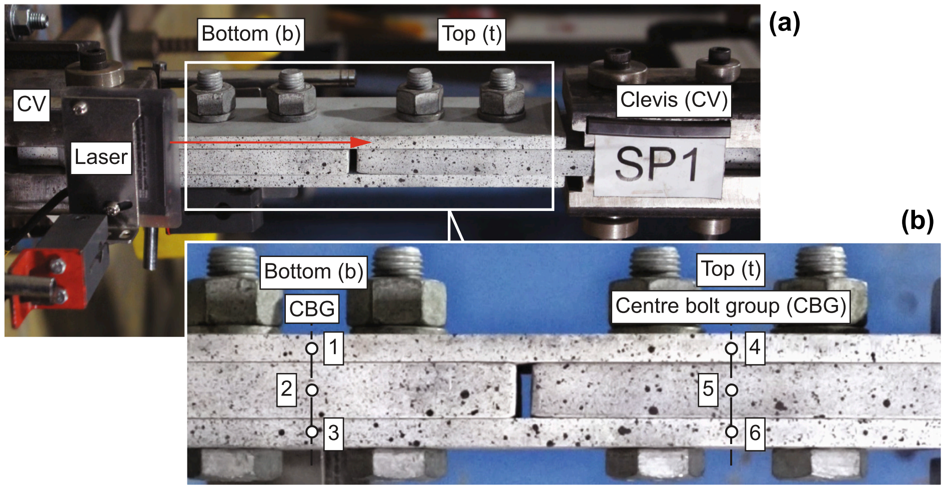

Fig. 5. (a) Still camera view of specimen and (b) video camera image showing points used for calculation of relative displacement (i.e., slip) via digital image correlation.

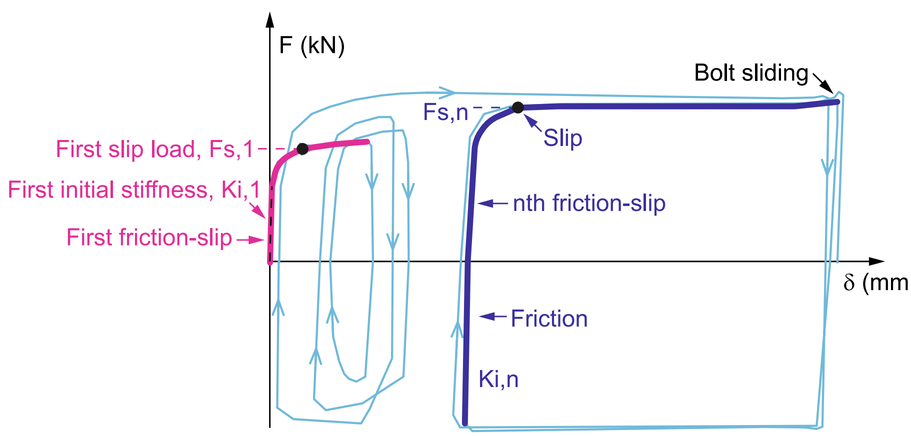

Fig. 6. Nominal force-slip behaviour showing first friction-slip and nth friction-slip.

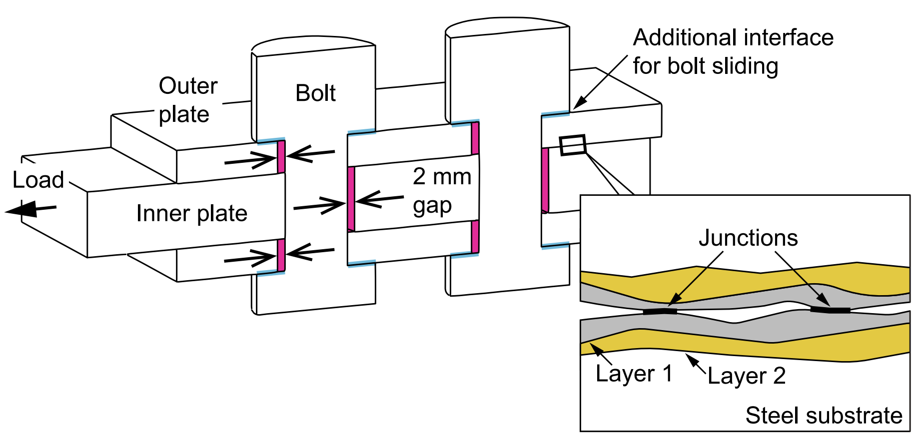

Fig. 7. Initial bolt hole tolerance and faying surface interface.

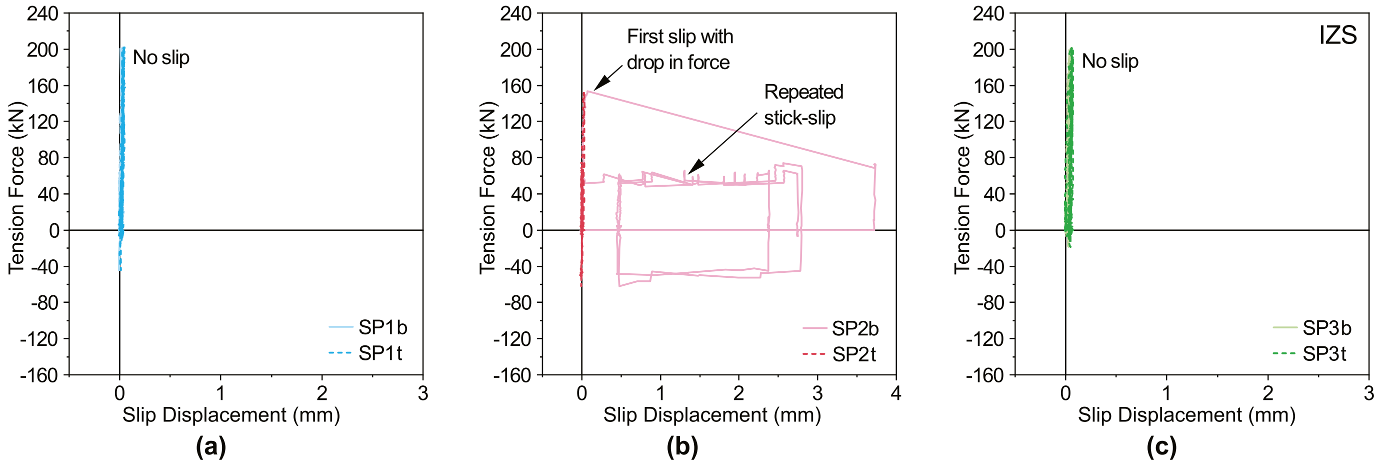

Fig. 8. Force-slip plots for IZS.

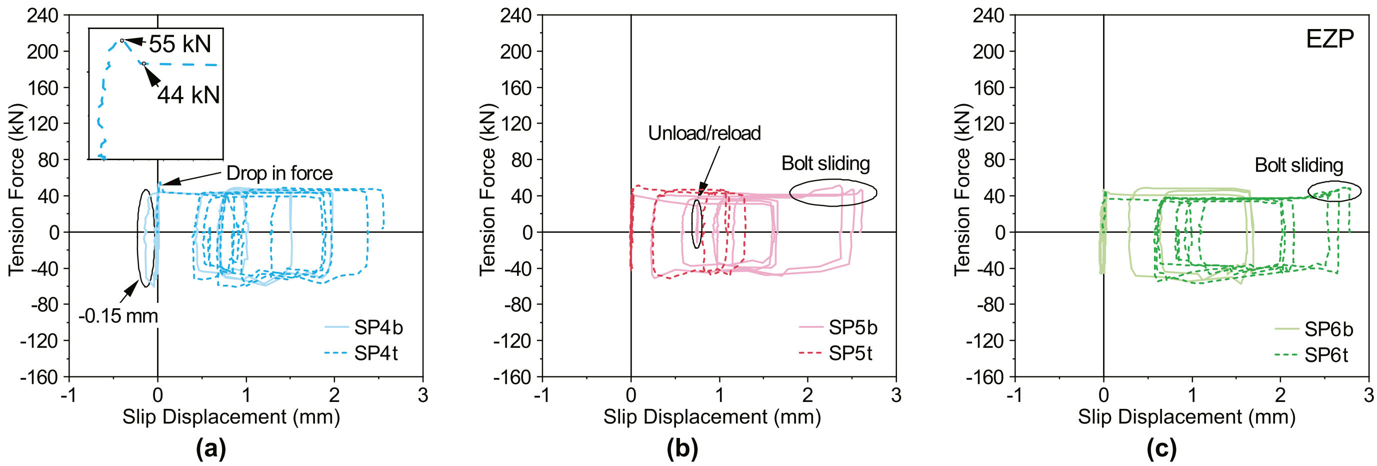

Fig. 9. Force-slip plots for EZP.

displacements. The relative displacements between the inner and outer plates (δ) were calculated as

$$\delta_{btm} = \frac{(y_1 - y_2) + (y_3 - y_2)}{2} = \frac{y_1 - 2y_2 + y_3}{2} \tag{2}$$

and

$$\delta_{top} = \frac{(y_5 - y_4) + (y_5 - y_6)}{2} = \frac{-y_4 + 2y_5 - y_6}{2}$$

where y_i was the time varying vertical displacement of each point i (Fig. 5), and δ_{btm} and δ_{top} were the average relative displacements at the bottom and top, respectively.

3.1. Force-slip behaviour

The general force-slip behaviour (Fig. 6) can be described as follows. The first friction-slip stage was characterised by the first slip factor and the first initial stiffness, as discussed in §3.2 and §3.3, respectively. The subsequent sliding cycles damaged the surfaces which affected the friction-slip behaviours, and the corresponding cumulative-displacement dependent slip factor and initial stiffness are discussed in §3.4 and §3.5, respectively.

Generally, friction at the inner/outer plate interfaces provided a substantial slip resistance with corresponding small relative displacements, hence, producing a high initial force-slip (F-δ) stiffness. When the applied force exceeded the friction resistance, there was a large relative displacement between the inner and outer plates. The inner plate slid, extending the length of the specimen, until the initial nominal 2 mm (average 2.3 mm) bolt hole tolerance was taken up, and the inner plate contacted the bolt shank (Fig. 7). The inner plate and the two bolts could then continue to slide together a further 2 mm (i.e., the nominal bolt hole tolerance for the outer plates). Continued sliding, however, required an increase in the applied force due to additional friction generated between the outer plates and each bolt head and nut (i.e., additional interface in Fig. 7).

Each specimen consisted of two connections (i.e., two groups of 2-M16 bolts) which could slip independently. Hence, the distribution of the displacement between the two ends of the specimen (i.e., top and bottom) was unknown prior to each test. It could be stated, however, that the sum of the relative displacement at each end ($\delta_{btm} + \delta_{top}$) was equal to the applied displacement ($d_{applied}$), less any losses due to elastic displacement of the clevises and bolts, and slip between the rig and specimen:

$$\delta_{btm} + \delta_{top} = d_{applied} + d_{losses} \tag{3}$$

Consider, for example, a 4 mm displacement cycle. If each end of the specimen had similar stiffness and slip resistance, then the relative displacement at each end might be equal (e.g., 1.875 mm assuming 0.125 mm loss). Equal distribution cannot be assumed, however, and in other circumstances the 4 mm displacement may be distributed as 1.75 mm at one end and 2.25 mm at the other end. This might occur, for example, if one end has greater slip resistance than the other end. In this

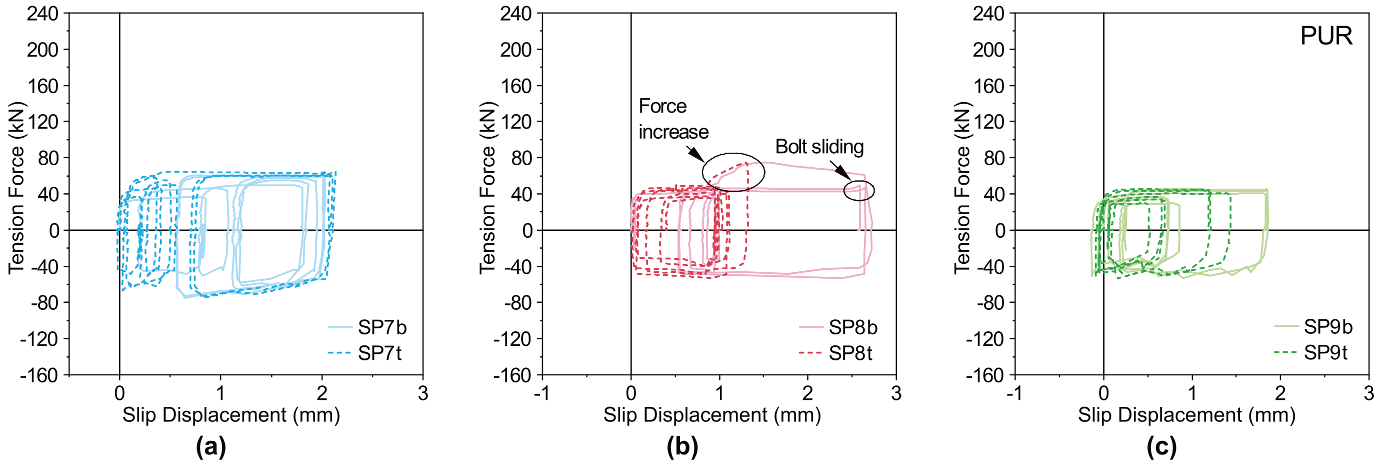

Fig. 10. Force-slip plots for PUR.

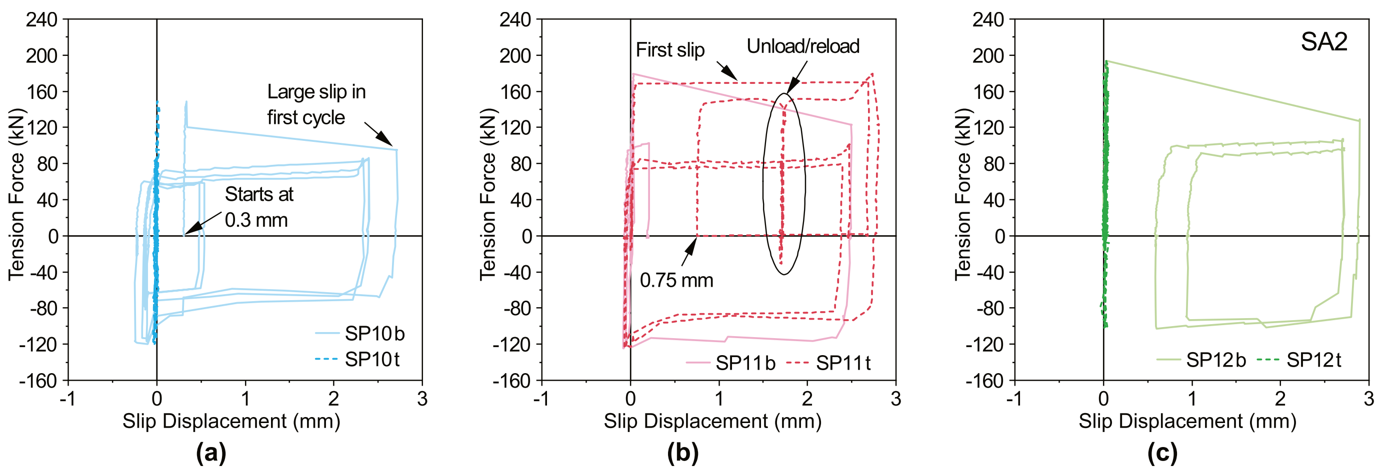

Fig. 11. Force-slip plots for SA2.

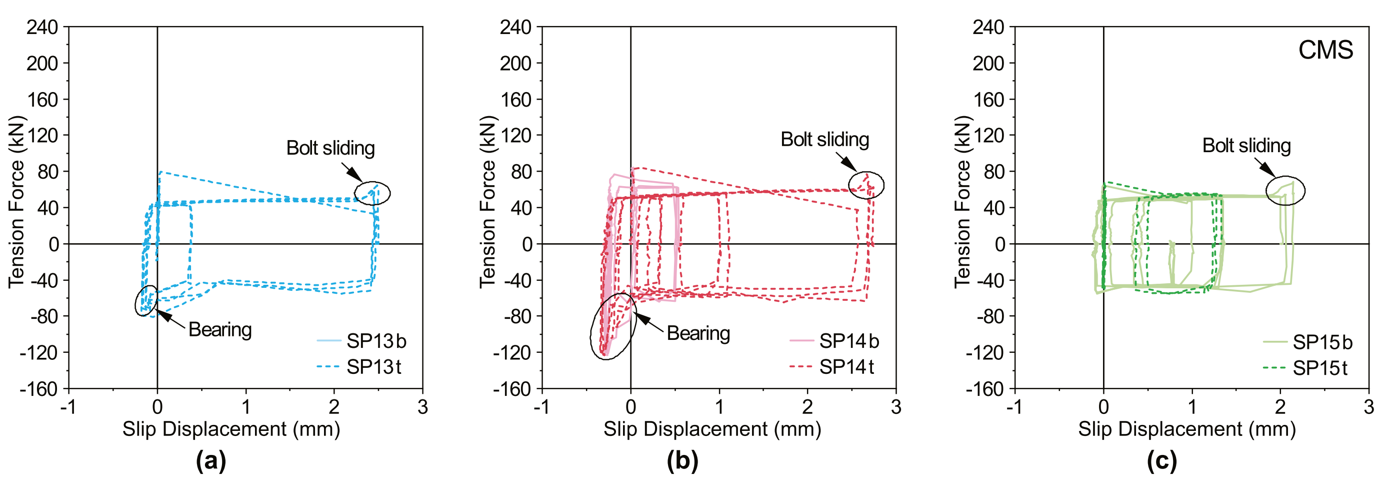

Fig. 12. Force-slip plots for CMS.

case, some increase in the force would be expected around 2 mm, as the bolt head and nuts begin sliding along the outer plates generating additional frictional resistance (e.g., bolt sliding in Fig. 6). Alternatively, one end of the specimen may have an actual bolt hole tolerance >2 mm, such that bolt sliding does not occur. In these ways, the resulting force-slip behaviours may not follow exactly the applied displacements.

The specific force-slip behaviours observed in this study can be described as follows. **IZS** specimens SP1 (Fig. 8a) and SP3 (Fig. 8c) did not slip before the test was terminated with a maximum force of 200 kN (i.e., the load cell capacity). SP2 (Fig. 8b) had a smaller bolt preload than SP1 and SP3 (63.3 kN cf. 95 kN), hence, the slip resistance was smaller, and slip was observed, although only at one end of the specimen. The

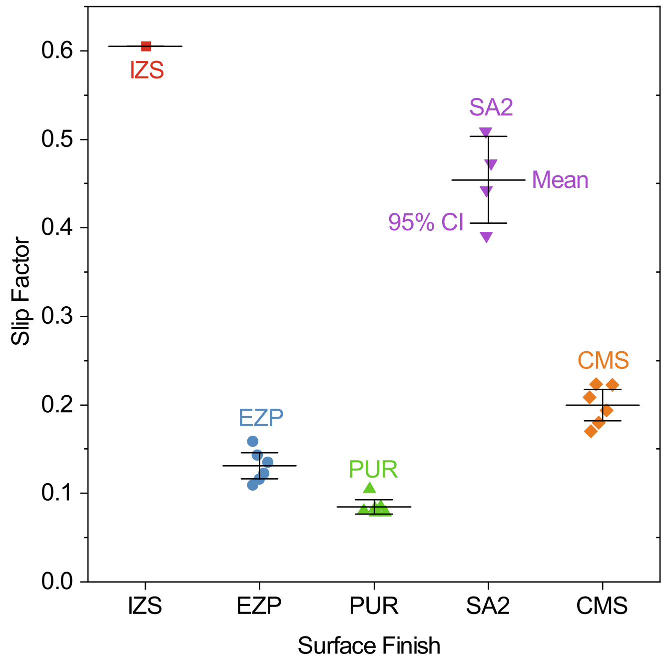

Fig. 13. First slip factor showing the mean and 95% confidence intervals (95% CI) for each surface finish.

Table 2
First slip load, slip factor, and initial stiffness for bottom (b) and top (t) of each specimen.

Ref.	Surface finish	First slip load, $F_{s,1}$ (kN)	Initial bolt tension, $F_{p,C}$ (kN)	First slip factor, $\mu_1 = \frac{F_{s,1}}{4F_{p,C}}$	First initial stiffness, $K_{i,1}$ (kN/mm)
SP1b	IZS	–	95	–	7,222
SP1t	IZS	–	95	–	7,662
SP2b	IZS	153.3	63.3	0.605	6,533
SP2t	IZS	–	63.3	–	6,445
SP3b	IZS	–	95	–	8,456
SP3t	IZS	–	95	–	7,973
SP4b	EZP	60.48	95	0.159	4,953
SP4t	EZP	54.71	95	0.144	4,435
SP5b	EZP	41.71	95	0.110	3,760
SP5t	EZP	51.44	95	0.135	3,693
SP6b	EZP	44.27	95	0.116	4,689
SP6t	EZP	46.82	95	0.123	4,485
SP7b	PUR	31.38	95	0.0826	4,927
SP7t	PUR	32.09	95	0.0844	5,329
SP8b	PUR	39.66	95	0.104	5,286
SP8t	PUR	30.46	95	0.0802	5,075
SP9b	PUR	29.65	95	0.0780	5,286
SP9t	PUR	29.65	95	0.0780	5,075
SP10b	SA2	148.7	95	0.391	13,390
SP10t	SA2	–	95	–	13,390
SP11b	SA2	179.8	95	0.473	14,090
SP11t	SA2	168.4	95	0.443	13,580
SP12b	SA2	193.6	95	0.510	13,940
SP12t	SA2	–	95	–	14,390
SP13b	CMS	73.62	95	0.194	6,683
SP13t	CMS	79.19	95	0.208	5,132
SP14b	CMS	84.80	95	0.223	5,893
SP14t	CMS	84.45	95	0.222	5,708
SP15b	CMS	64.63	95	0.170	6,231
SP15t	CMS	68.39	95	0.180	5,715

Note: The missing values (i.e., "-") reflect specimens which did not slip; hence, the slip factor could not be calculated.

bottom end of SP2 (i.e., SP2b) slipped suddenly and the impact as the bolts came into bearing caused a loud noise and the laser displacement sensors to fall. Consequently, the test was stopped and restarted after the first slip. When the connection first slipped, the applied force dropped from 153 kN to 69 kN (i.e., 55% reduction). This drop in force may have occurred for three reasons. Firstly, when the friction resistance was exceeded, the specimen length suddenly increased, releasing hydraulic pressure on the piston in the return stroke and, hence, reducing the applied force. Secondly, sliding of the specimen plates could have led to the change from the higher static friction coefficient to the lower dynamic (kinetic) friction coefficient. That is, the high sliding velocity could lead to a reduced friction resistance due to a reduction of the friction coefficient from the static to the dynamic value. Thirdly, the initial sliding may have damaged the faying surfaces resulting in a reduction of the effective friction coefficient. For example, the process of sliding could result in flattening of the surface asperities which were initially interlocking on a rough surface. In the later cycles, the force-slip curve was characterised by a repeated stick-slip behaviour (Fig. 8b).

All the **EZP** coated specimens slipped at each end during the tests (Fig. 9). The force-slip curves were smooth, and the frictional behaviour was less severe than the IZS specimens. A drop in force was observed following the first slip of each connection. SP4t, for example, quickly dropped from 55 kN to 44 kN, and further reduced to 39 kN by the end of the tension load cycle (i.e., 30% reduction). SP4b first slipped during a compression load cycle indicating 0.15 mm initial misalignment (Fig. 9a). SP5b had one unload/reload cycle due to experimental error (Fig. 9b). Bolt sliding was observed in the force-slip plots for SP5b and SP6t (Fig. 9b,c).

The **PUR** specimens displayed a smooth force-slip curve with a gradual increase in the slip displacement approaching the slip resistance (Fig. 10), and there was no substantial drop in force when the specimens slipped. The results indicated a lower post-slip sliding velocity with no substantial change in the friction coefficient from the initial static value. For the cyclic behaviour, however, the force-slip plots showed a gradual increase in the slip resistance with each cycle. For SP8, an increase in the force to 75 kN was observed during the first 4 mm cycle (Fig. 10b). The reason for this uncharacteristic increase in load (cf. earlier cycles) cannot be given definitively, however, as it may be related to a change in the faying surface due to damage, or due to sliding of the bolts. The SP8t force-slip plot starts at 0.4 mm as the bolt shank was not completely pushed to one side of the bolt hole (i.e., experimental error). The onset of bolt sliding in SP8b occurred at 2.5 mm (Fig. 10b), i.e., 0.2 mm greater than the average 2.3 mm tolerance.

The **SA2** specimens displayed a severe frictional behaviour with a high slip resistance, a sudden increase in the slip displacement and an associated drop in the force (Fig. 11). SP11b, for example, had a slip resistance of 180 kN, which dropped to 123 kN at the end of the tension cycle (i.e., 32% reduction). The SP10b force-slip plot (Fig. 11a) starts at 0.3 mm as the bolt shank was not completely pushed to one side of the bolt hole (i.e., experimental error). Moreover, SP10 was inadvertently loaded to a large slip displacement in the first cycle. The slip occurred quickly and caused some damage to the bolt threads. When SP11 first slipped, the shock caused the laser displacement sensor to fall and the test was stopped. The test was continued after the laser was reattached. The bolt position was not reset completely for SP11t such that the force-slip curve begins at 0.75 mm for the second part (Fig. 11b). One unload/reload cycle was incorporated and gave another measurement of the slip factor and initial stiffness for slightly larger cumulative displacement (Fig. 11b).

The **CMS** specimens displayed a moderate frictional behaviour (Fig. 12). The slip resistance was less than that of the IZS and SA2 specimens, however, a substantial drop in load was observed following the slip. SP13t, for example, reached 79 kN in the first cycle before falling to 33 kN (i.e., 58% reduction). SP13t, SP14t, and SP15b all displayed bolt sliding in the force-slip plots (Fig. 12). The plots for SP13t and SP14 show an increase in the force-slip stiffness due to bearing. This

Table 3
Standard calculation of slip factor for design purposes.

Surface finish	Sample size, n	Mean slip factor, μ_m	Standard deviation, s_μ	95% Confidence interval (Eq. (5)) (% of mean)	Coefficient, k_p (Eq. (6))	Characteristic slip factor, μ_{EN} (Eq. (6))	Coefficient, k (Eq. (7))	AS 4100 slip factor, μ_{AS} (Eq. (7))
IZS	1	0.605	–	–	–	–	–	–
EZP	6	0.131	0.0184	± 0.0148 (± 11.2%)	2.34	0.0882	0.85	0.110
PUR	6	0.0846	0.0100	± 0.00801 (± 9.47%)	2.34	0.0612	0.85	0.0780
SA2	4	0.454	0.0500	± 0.0490 (± 10.8%)	2.68	0.320	0.85	0.391
CMS	6	0.200	0.0221	± 0.0177 (± 8.85%)	2.34	0.148	0.85	0.170

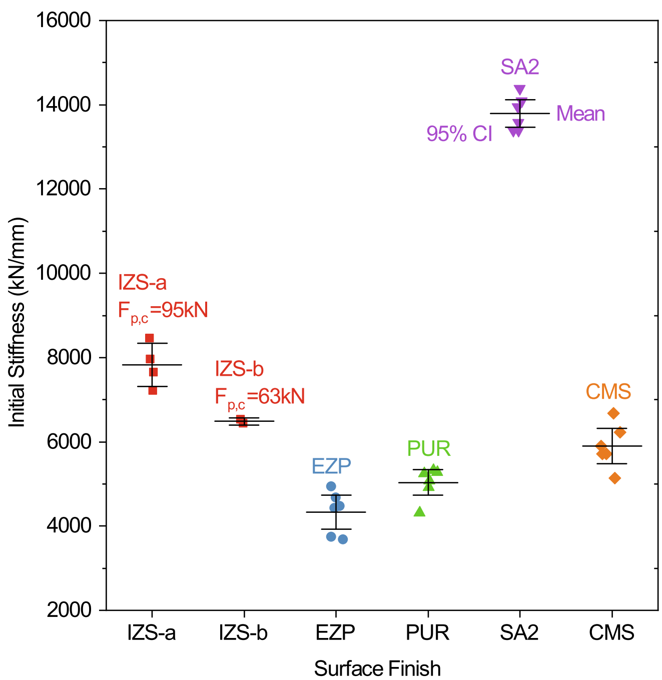

Fig. 14. First initial stiffness showing the mean and 95% confidence intervals (95% CI) for each surface finish.

occurred when the specimens were accidently shortened beyond their initial lengths, such that the plates were constrained by the bolt shanks, resulting in an increase in the force-slip stiffness.

3.2. First slip factor

The first slip load ($F_{s,1}$ in Fig. 6) was identified for each specimen as either the slip load at a slip displacement of 0.15 mm, or the earlier peak force prior to slip, i.e., sudden increase in the slip displacement (Fig. 13, Table 2). The first slip factors were determined as

$$\mu_1 = \frac{F_{s,1}}{4F_{p,C}} \tag{4}$$

where $F_{s,1}$ was the first slip load, and $F_{p,C}$ was the initial bolt tension. A lower bound was suggested when slip did not occur before the loading was terminated at a maximum of 200 kN (i.e., $\mu_1 > 0.5263$).

The mean and 95% confidence intervals were calculated for each of the surface finishes (Fig. 13, Table 3). The 95% confidence interval was calculated as [22]

$$\mu_m \pm z_{\alpha/2}\frac{s_\mu}{\sqrt{n}} \tag{5}$$

where n was the number of individual slip factor values, μ_m was the mean, $s_\mu = \sqrt{\frac{\sum(\mu_i-\mu_m)^2}{n-1}}$ was the sample standard deviation, and $z_{\alpha/2}$ was the z-value leaving an area of $\alpha/2$ to the right of the normal distribution, e.g., $z_{0.025} = 1.96$ for the 95% confidence interval [22]. This assumed that the sample size was large enough that the sample standard deviation was close to, and could be substituted for, the true standard deviation of the population (σ_μ) [22]. The variation of the mean first slip factor indicated by the confidence interval for each surface finish can be attributed to the variation of the bolt preload (see §2.1), substrate material properties and preparation, and coating material properties and geometry (i.e., surface profile and coating thickness).

For design purposes, a 5% fractile with specified confidence might be preferred over the mean or confidence interval. Considering EN 1090–2 [6], for example, the characteristic slip factor (μ_k) can be calculated based on the p-fractile with γ confidence level as [23]

$$\mu_{EN} = \mu_k = \mu_m - k_p s_\mu \tag{6}$$

where the coefficient k_p ($p = 0.05$, $\gamma = 0.75$) equals 2.05 provided that five specimens are tested yielding ten values (i.e., $n = 10$) [6]. For other sample sizes, k_p must be determined otherwise. Applying the coverage method [23], for a normally distributed population with unknown standard deviation, the coefficients for the lower 5%-fractile with confidence $\gamma = 0.75$ are $k_p = (3.15, 2.68, 2.46, 2.34, 2.19)$ for $n = (3,4,5,6,8)$. Thus, μ_{EN} was calculated (Table 3) such that k_p accounted for the sample size without any assumption regarding the sample and population standard deviations (as was required for the confidence interval).

In contrast, for AS 4100 [24], the design slip factor is calculated as

$$\mu_{AS} = k\left(\mu_m - 1.64s_\mu\right) \geq \mu_{i,min} \tag{7}$$

where $\mu_{i,min}$ is the minimum individual μ value, μ_m is the sample mean, s_μ is the sample standard deviation, and k is 0.85 when 3 specimens are tested, or 0.90 for 5 or more specimens. ($\mu_m - 1.64s_\mu$) represents the 5% fractile with 75% confidence level for an infinite sample size, while the k-factor corrects for the actual sample size. In the present study, Eq. (6)

Table 4
Mean and characteristic first initial stiffness.

Surface finish	Sample size, n	Bolt preload (kN)	Mean initial stiffness (kN/mm)	Standard deviation (kN/mm)	Coefficient, k_p (Eq. (6))	Characteristic initial stiffness (kN/mm)
IZS-a	4	95	7,830	520	2.68	6,440
IZS-b	2	63.3	6,490	62.1	–	–
EZP	6	95	4,340	506	2.34	3,150
PUR	6	95	5,160	160	2.34	4,790
SA2	6	95	13,800	408	2.34	12,800
CMS	6	95	5,890	526	2.34	4,660

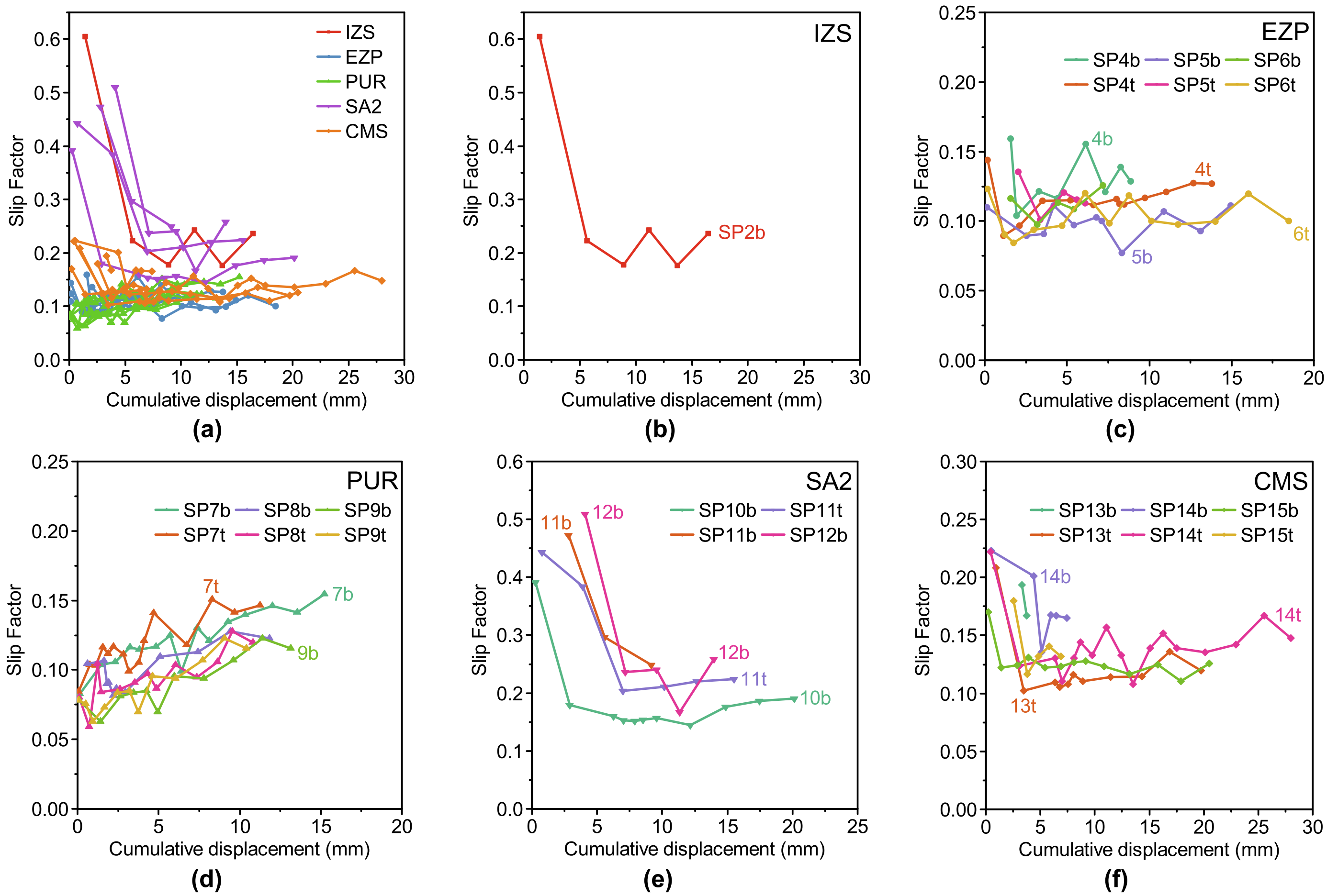

Fig. 15. Variation of slip factor during cyclic loading showing (a) all specimens, (b) IZS, (c) EZP, (d) PUR, (e) SA2 and (f) CMS surface finishes.

gave slightly different slip factors compared with Eq. (7) (Table 3). The difference was mainly due to the lower limit $\mu_{i,min}$ in Eq. (7), which determined μ_{AS} in each case and resulted in μ_{AS} being 15% to 30% higher than μ_{EN} (Table 3).

3.2.1. Comparison with existing studies

The existing studies for steel surfaces were outlined in the introduction with reference to the authors previous work [4]. For the coated steel, a number of existing studies have considered the short term slip resistance based on quasi-static monotonic tests. Kulak et al. [25] reported average slip factors for organic zinc-rich coated surfaces ranging between 0.2 and 0.47 depending on the coating type, thickness, and surface preparation. In contrast, zinc silicate coatings were reported to have slip factors ranging between 0.50 and 0.68, and the higher values were attributed to the greater hardness of the inorganic zinc silicate coating. In another study Cruz et al. [26] reported the slip factor for mild steel (S 275) joints determined using the EN 1090–2 method, including surfaces sand blasted with degree Sa 2.5 and subsequently coated with either 70 μm zinc ethyl-silicate or 70 μm zinc epoxy. The mean slip factors were given as 0.457 and 0.378 for the ethyl-silicate and epoxy coatings, respectively. A thicker 135 μm zinc epoxy coating was also applied to high strength steel (S 690) which resulted in a lower mean slip factor of 0.244. Overall, it was concluded that the slip factor was strongly affected by the surface treatment and weakly affected by the steel grade.

Tamba et al. [27] investigated the slip factor for specimens with roughened steel surfaces and inorganic zinc-rich coatings. The test method was similar to Annex G of EN 1090–2 except that M22 grade F10T bolts were used to join the SS400 steel plates which had yield strengths of 287 MPa and 265 MPa for the 28 mm and 16 mm thicknesses, respectively. Four specimens had each faying surface coated with 75 μm of inorganic zinc-rich paint, while a further 30 specimens had faying surfaces composed of one painted surface and one uncoated roughened steel surface. The preparation of the roughened steel surface varied using different power tools, e.g., disc sander, wire brush, and blast cleaning, which gave different surface roughness measurements. The four specimens with 75 μm inorganic zinc-rich paint gave slip factors of 0.60 to 0.70. With one roughened surface prepared by blast-cleaning to an average maximum height roughness of 70 μm and the other surface coated with 75 μm inorganic zinc primer, the slip factor varied between 0.57 and 0.64.

When the uncoated steel roughness measurement was less than the dry film thickness of the coating, the slip factor increased linearly with the roughness measurement. However, when the roughness was greater than the coating thickness, the slip factor was smaller than that indicated by the linear trend. This was explained with reference to the failure mechanism which was determined by observation of the post-test faying surfaces. When the surface roughness was small, e.g., average maximum height of roughness <50 μm, although the coated surface was damaged, the paint was not well adhered to the substrate and the failure occurred at the steel-paint interface, i.e., interfacial failure. In contrast, when the surface roughness was large, e.g., >50 μm, the paint adhesion to the substrate was enhanced, and the failure occurred in the paint film, i.e., cohesion failure. Overall, the findings indicate that the slip factor of coated specimens can be strongly affected by the steel surface roughness and, hence, the steel grade since it affects the surface roughness obtained from the blast cleaning process, for example.

Wang et al. [28] studied the slip factor of high strength steel (Q345,

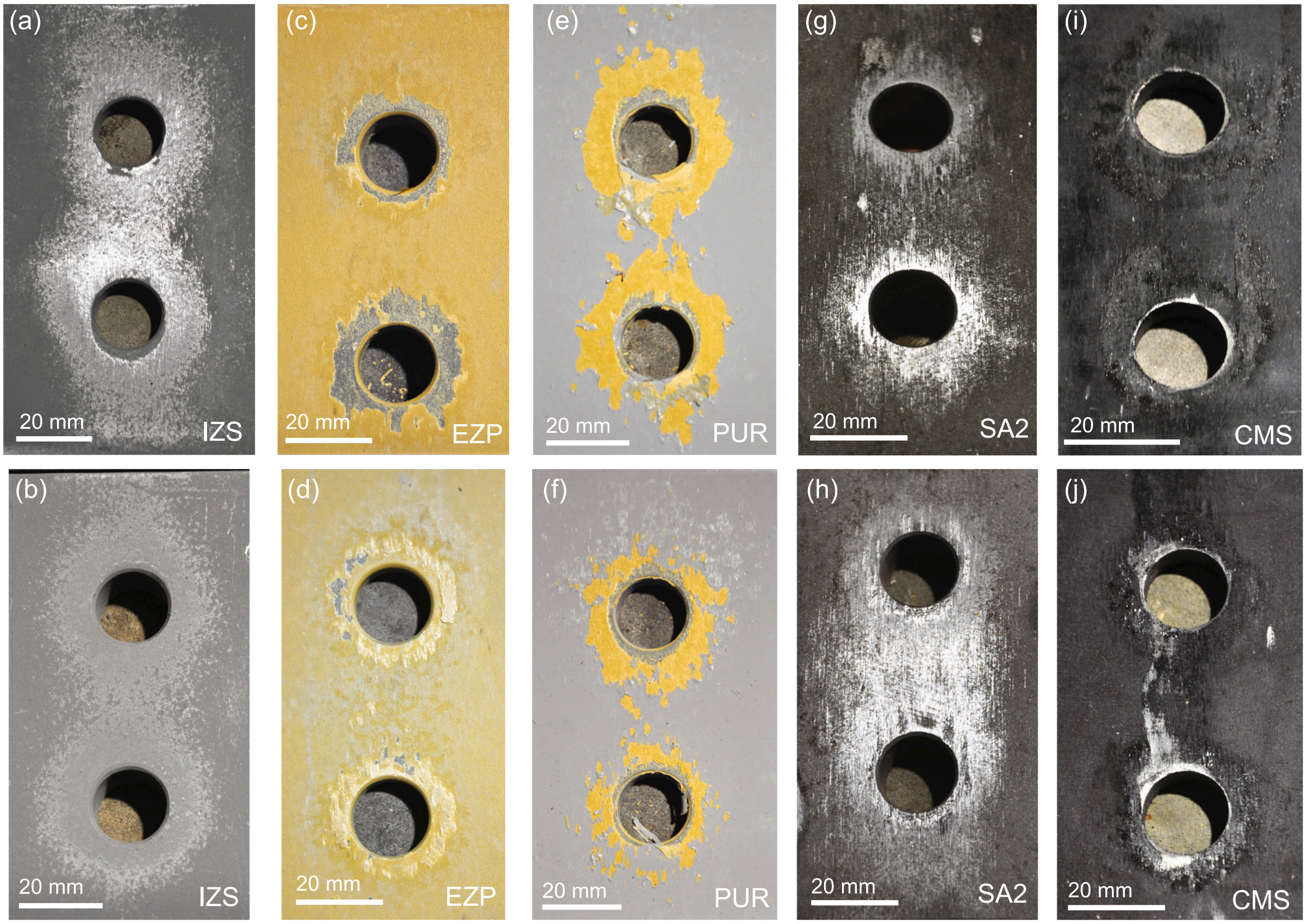

Fig. 16. Post-test faying surfaces indicating the range of surface condition for each surface finish.

Q550, Q690 and Q890) with an inorganic zinc-rich coating and carried out tests in accordance with Annex G of EN 1090–2. The short-term mean slip factors varied between 0.333 and 0.365 depending on the steel grade and the coating thickness (60 or 80 μm). Generally, higher surface roughness was obtained when sand blasting steel with lower strength and hardness. Enhanced mechanical interlock of the rougher faying surfaces yielded greater slip resistance and, hence, greater slip factor. Wang et al. [28], however, illustrated that the zinc-rich coating separates the roughened steel surfaces resulting in a lower slip factor compared to the uncoated material and a weakened dependence of the slip factor on the high strength steel grade. On the other hand, the coating thickness had a more substantial effect, with 80 μm inorganic zinc-rich coated specimens having slip factors generally 10% greater than those with only 60 μm thickness.

In the present study, only one estimate of the **IZS** slip factor was obtained (0.61), which matched those in the existing literature well, e.g., 0.50 to 0.68 [25]. The **EZP** slip factors (0.11 to 0.16, $\mu_m = 0.13 \pm 0.015$, $n = 6$), however, were low compared with those in the existing literature, e.g., 0.2 to 0.47 [25]. The **PUR** slip factors were also relatively low (0.078 to 0.10, $\mu_m = 0.085 \pm 0.0080$, n = 6); however, no slip factors were found in the existing literature for comparison. The present **SA2** slip factors (0.39 to 0.51, $\mu_m = 0.45 \pm 0.049$, $n = 4$) can be compared with the values from the previous study [4], i.e., **SA1** (0.50 to 0.60, $\mu_m = 0.55 \pm 0.031$, $n = 5$) and **SA3** (0.51 to 0.61, $\mu_m = 0.55 \pm 0.035$, n = 5). SA1, SA2, and SA3 represent increasing cleanliness of the substrate according to AS 1627.4 [7]. If the slip factor varied only due to the cleaning process, then the SA2 slip factor might fall between the SA1 and SA3 values. However, the present SA2 slip factors were less than the previous values, despite the use of the same equipment and similar procedures. Hence, the degree of sandblasting determined by visual assessment may not be a reliable indicator of the slip factor. Additionally, the present SA2 slip factors were more variable than in the previous study, i.e., $s_\mu / \mu_m = 11\%$ (SA2) cf. 6.4% (SA1) and 7.2% (SA3), mainly due to one low value in the present study. Similarly, the present **CMS** slip factors (0.17 to 0.22, $\mu_m = 0.20 \pm 0.018$, n = 6) may be compared with the previous slip factors [4] (0.27 to 0.36, $\mu_m = 0.31 \pm 0.015$, $n = 9$). The present CMS slip factors were again lower than the previous values, which may be due to differences in the mill scale layer composition and condition.

The applications for structural analysis and design are discussed in §4. For the coated steel, with substrate surface roughness of 70 to 75 μm, the first slip factor was generally controlled by failure in the paint film. Hence, the results were consistent with the findings of Tamba et al. [27], and indicated satisfactory paint adhesion to the substrate. The cyclic loading, however, led to damage of the paint coating and exposed the steel substrate. The slip behaviours of the later cycles were therefore determined by the interaction between the steel substrates, which was influenced by the remaining paint fragments in some cases (refer §3.4 and §3.5). Additionally, as the friction resistance was exceeded the plates began to slip, and this relative displacement damaged the paint coatings. Consequently, the load drop after first slip may also have been influenced by the nature of the steel substrates. For the IZS coating, the present results contradict the findings of Wang et al. [28] by indicating a higher slip factor for the coated material compared with the uncoated material.

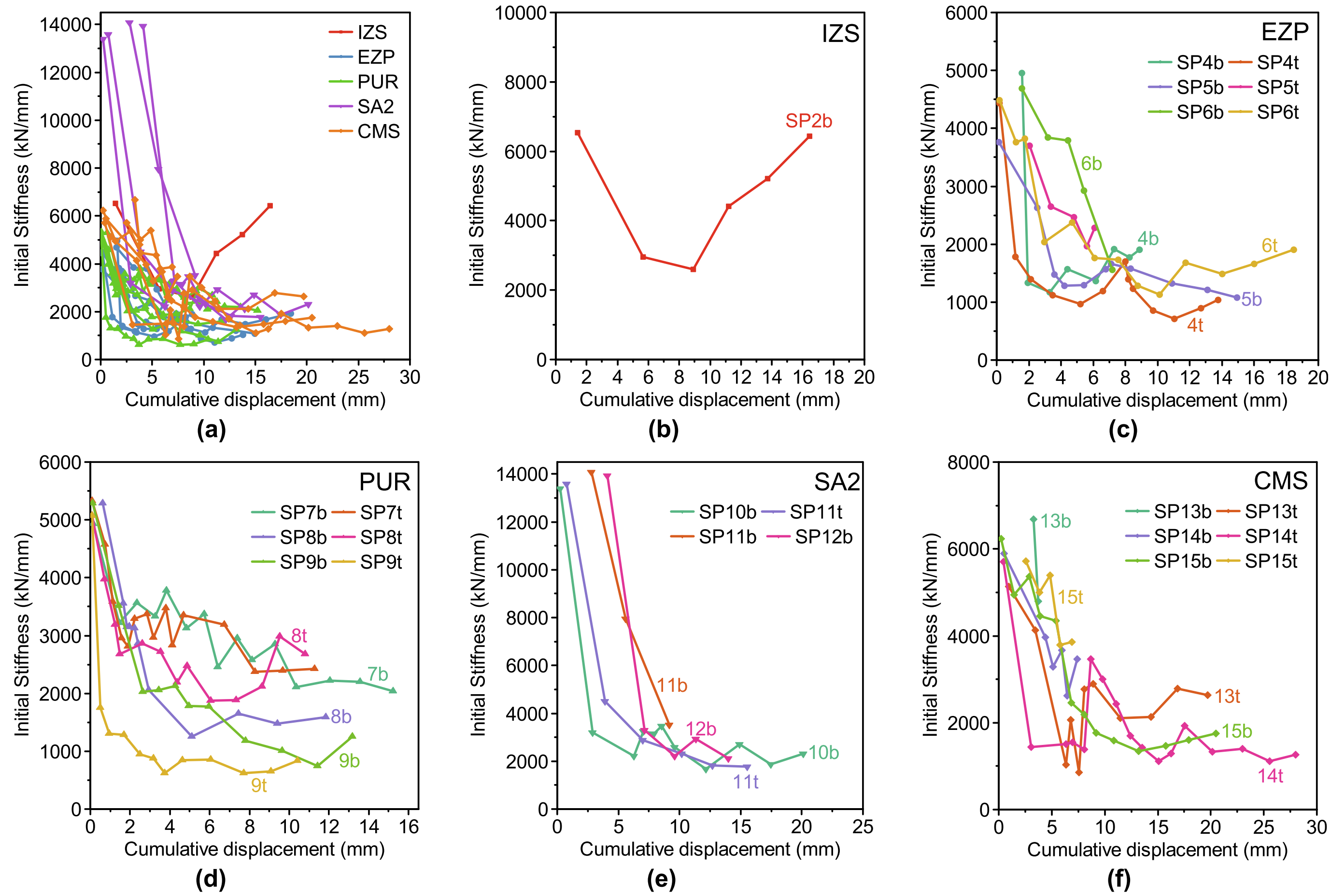

Fig. 17. Variation of initial stiffness during cyclic loading showing (a) all specimens, (b) IZS, (c) EZP, (d) PUR, (e) SA2 and (f) CMS surface finishes.

3.3. First initial stiffness

The first initial stiffness ($K_{i,1}$, Fig. 6) was identified by inspection of the force-slip plots for each specimen (Table 2, Fig. 14) and the mean and characteristic values were calculated (Table 4). The SA2 specimens had the highest initial stiffness (13,800 kN/mm), followed by the IZS specimens, for which the initial stiffnesses were 7,830 and 6,490 kN/mm for the bolt preloads of 95 kN and 63.3 kN, respectively. The EZP, PUR, and CMS specimens had the lowest stiffnesses of 4,340, 5,160, and 5,890 kN/mm, respectively. For comparison, the previous study [4], which had the same bolt preloads as the present study (95 kN), gave initial stiffnesses of 14,900, 18,600, and 18,600 kN/mm for the CMS, Sa1 and Sa3 specimens, respectively. Hence, the present stiffnesses were generally less than those in the previous study [4].

3.4. Cyclic slip factor

For each specimen, the slip load and, hence, slip factor was determined for each load cycle based on the initial bolt preload. The slip factor could vary due to changes in the bolt preload and due to degradation of the faying surface, both of which were incorporated in the reported slip factor variation. The absolute value of the applied force was adopted so the resulting slip factors were all positive. For a given specimen, the number of measurements of the slip resistance was in the range of $0 \leq N \leq 18$, where the maximum value was equal to twice the number of cycles according to the loading protocol. The slip number, i.e., $n = 1, 2, 3, \ldots, N$ for each subsequent slip, gave limited information on the potential degradation of the faying surfaces due to the prior slip displacements, and was highly dependent on the loading protocol and also on the specific slip sequence. Therefore, the cumulative displacement, a better measure of the progressive degradation, was adopted for correlation with the varying slip factor. The cumulative displacement at the jth time step (Δ_j) was defined as

$$\Delta_j = \sum_{i=1}^{j} |\delta_i - \delta_{i-1}| \tag{8}$$

where $i = 1, 2, \ldots, j$ were the time steps and δ_i was the slip (i.e., relative displacement) at the ith time step such that $\delta_0 = 0$. With this definition the first slip could occur at a small cumulative displacement (e.g., 0.1 mm) if the connection slipped on the first cycle, or a larger cumulative displacement (e.g., 5 mm) if the connection was subjected to several cycles before the slip resistance was exceeded.

For the **IZS** specimens, only SP2b slipped (Fig. 15b), however, the slip factor quickly reduced (0.6 to 0.2) with the increasing cumulative displacement (Δ). This reduction can be explained with reference to the post-test faying surfaces (Fig. 16). Initially, the IZS coating separated the steel substrates, resulting in a high slip factor. The post-test faying surfaces of specimens which did not slip during the test (e.g., Fig. 16b) showed the paint coating was smoothed around the bolts but remained adhered to the steel substrate. For the specimen which slipped, however, the coating was damaged exposing the underlying steel which was smoothed and shiny (Fig. 16a). The steel substrate was sand blasted prior to painting and was smoothed only due to the test. This suggests that the larger cumulative displacement (Δ) damaged the surface coating, thereby exposing the underlying steel and giving a reduced slip factor due to the lesser friction coefficient of the smoothed steel compared with the initial IZS coated surface. If the cyclic loading was continued, further reduction of the slip factor might occur due to continued polishing of the steel substrate, although this was not

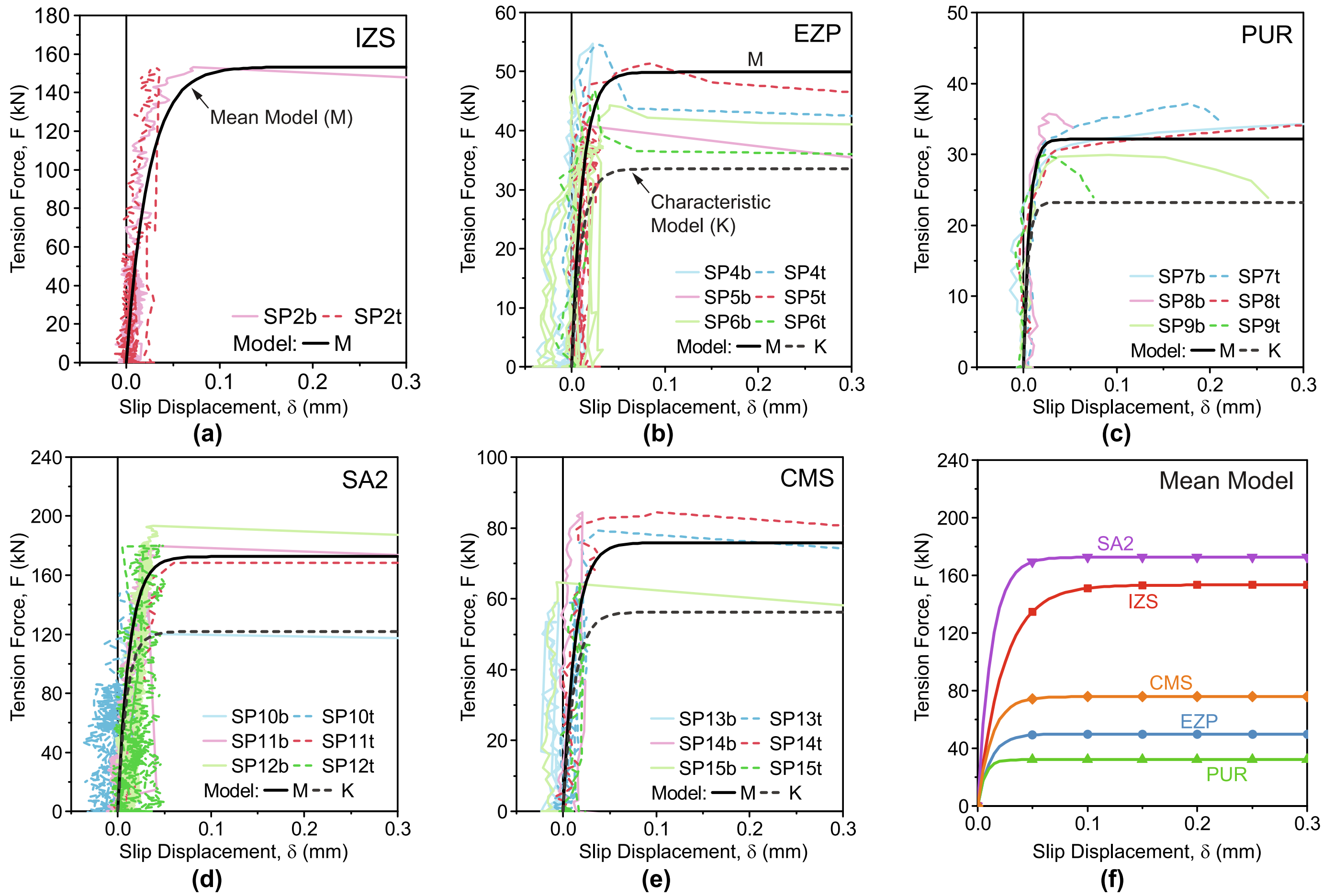

Fig. 18. Simplified model: (a) IZS, (b) EZP, (c) PUR, (d) SA2, (e) CMS, and (f) Simplified model (mean).

Table 5
Simplified model parameters including slip resistance (Fs) and initial stiffness (Ki).

		Mean (M)		Characteristic (K)	
Surface finish	Bolt preload (kN)	Fs (kN)	Ki (kN/mm)	Fs (kN)	Ki (kN/mm)
IZS-a	95	–	7,830	–	6,440
IZS-b	63.3	153	6,490	–	–
EZP	95	49.9	4,340	33.5	3,150
PUR	95	32.1	5,160	23.2	4,790
SA2	95	173	13,800	122	12,800
CMS	95	75.8	5,890	56.2	4,660

demonstrated by the present test.

The first mean slip factor for the **EZP** specimens was 0.13. The slip factor reduced slightly after the first slip (0.13 to 0.10), and then displayed a very slight increase with the increasing cumulative displacement, Δ (Fig. 15c). The post-test faying surfaces showed that the coating was well adhered, hence, the relatively low first mean slip factor may be associated with the EZP coating which initially separated the steel substrates. In some cases, the paint coating was damaged in patches and the substrate was barely exposed (Fig. 16d). In other cases, the coating was more extensively damaged, exposing the substrate around the perimeter of the bolt holes and leaving paint fragments (Fig. 16c). The exposed steel presented as a sandblasted surface, i.e., was not smoothed nor shiny, suggesting the remaining paint fragments had some lubricating effect, which might have contributed to the reduction of the slip factor after the first slip. The very slight increase in the slip factor with increasing Δ might be associated with a trend towards the smoothed steel slip factor of 0.2. That is, the slip factor may have increased slightly for some specimens due to shedding of the paint fragments which allowed partial contact between the steel substrates, thereby increasing the effective friction coefficient. With continued cyclic loading, a further increase in the slip factor might occur, i.e., from 0.1 to 0.2, due to continued shedding of the paint fragments which allows direct contact between the steel substrates.

The **PUR** specimens had a mean first slip factor of 0.085 and displayed an increasing trend with the increasing cumulative displacement, Δ (Fig. 15d). Some post-test faying surfaces showed portions of the PUR coating was damaged around the bolt holes exposing the underlying EZP layer, while the steel substrate was only exposed immediately around the perimeter of the bolt holes (Fig. 16f). In other cases the PUR coating was more extensively damaged around the bolt holes, and more of the steel substrate was exposed around the bolt hole perimeter (Fig. 16e). In both cases paint fragments were observed and the exposed steel also presented as a sandblasted surface. The slip factor generally increased from 0.085 to 0.13 (Fig. 15d) reflecting the slip factor for the EZP coating. Further cyclic loading might result in a further increase in the slip factor as the steel substrate was further exposed, however, this was not carried out in the present tests.

For the **SA2** specimens the slip factor quickly reduced from the mean value of 0.45, trending towards a value of 0.2 (Fig. 15e). The post-test faying surfaces showed a smoothed shiny surface around the bolt holes which was characterised by lines elongated in the direction of travel. For some specimens the smoothed areas were located closely around the bolt hole perimeters (Fig. 16g), while in other specimens a single larger smoothed area was observed (Fig. 16h). The post-test

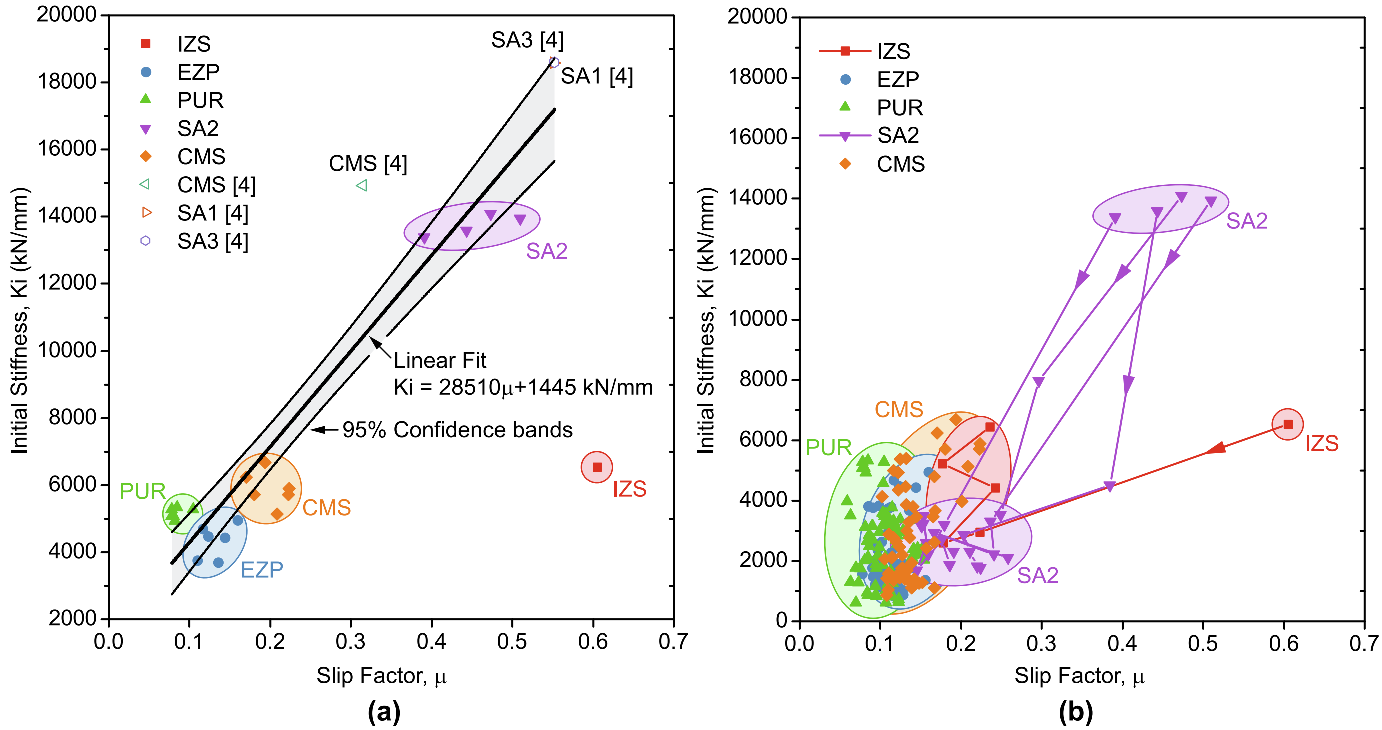

Fig. 19. Initial stiffness against slip load for (a) first slip and (b) all slips.

surfaces suggested that the high initial slip factor associated with the sand blasted surfaces was reduced as the sliding smoothed the steel surfaces, which occurred quickly after the faying surfaces began slipping.

The mean first slip factor for the **CMS** specimens was 0.2. The slip factor reduced after the first slip (~0.1), after which it slightly increased with the cumulative displacement, Δ (Fig. 15f). Some specimens had the slip factor increase, e.g., SP14t at Δ = 7.5 mm, then decrease again before following the gradual increasing trend again. The post-test surfaces showed that the mill scale layer was damaged, exposing portions of the underlying steel during the test. Some specimens had the mill scale layer damaged around the bolt holes (Fig. 16i), while other specimens showed some surface damage further away from the bolt holes (Fig. 16j), the latter being explained by variation in the mill scale surface profile. In both cases mill scale layer fragments were observed, and the exposed steel surfaces were smooth and shiny. The slip factor generally trended towards a value of 0.15, reflecting the smooth steel surface which was not sandblasted at any stage.

3.5. Cyclic initial stiffness

The cyclic initial stiffness was also identified for each load cycle by inspection of the force-slip plots, and the results were plotted against the respective cumulative displacements (Fig. 17). The results generally showed that the initial stiffness reduced with increasing cumulative displacement, irrespective of the variation of the slip factor with the cumulative displacement. This reflected the general smoothing of the faying surfaces, which occurred as the sliding progressed. The **EZP** and **CMS** specimens, for example, showed a reducing stiffness (Fig. 17c,f) despite the relatively constant slip factor (Fig. 15c,f). Similarly, the **PUR** specimens also displayed a reducing stiffness (Fig. 17d) despite the increasing slip factor (Fig. 15d). Notably, **IZS** specimen SP2b showed that, after the initial stiffness reduction, the stiffness could increase again (Fig. 17b), despite the relatively constant slip factor (Fig. 15b). Further testing is required to verify this behaviour, however, due to the low sample size ($n = 1$).

4. Applications for structural design and analysis

In the basic design case, the slip resistance is calculated based on the characteristic slip factor to ensure that the connection will not slip when subjected to the foreseen design actions. The slip factor might be selected from a design standard, or otherwise be based on specific slip factor tests. The present study provides slip factors for each surface finish (Table 3) which can be compared with the standard values. In AS 4100:2020 [24], for example, a slip factor of 0.35 is specified for clean "as-rolled" surfaces. For the CMS surface, however, the present results indicated a mean slip factor, $\mu_m = 0.20$, an EN 1090–2 characteristic value, $\mu_{EN} = 0.15$, and an AS 4100 design value of $\mu_{AS} = 0.17$. Indeed, even the previous study [4] indicated a slip factor <0.35, i.e., $\mu_m = 0.31$, and $\mu_{EN} = \mu_{AS} = 0.27$. Thus, the standard value of $\mu_{AS} = 0.35$ could be too high in some cases, and a lesser value of 0.20 is suggested for general design in the absence of more specific test results. This finding is consistent with EN 1090–2:2018 [6], which specifies a slip factor of 0.20 for surfaces as rolled.

Otherwise, EN 1090–2 indicates $\mu_{EN} = 0.40$ for blasted surfaces coated with alkali-zinc silicate paint with a nominal thickness of 70 μm (40 μm to 80 μm). Such surfaces are designated class B and the slip factor is expected to fall in the range of $0.40 \leq \mu_{EN} \leq 0.50$ (with $\mu_{EN} = 0.40$ for design purposes). In comparison, the present study found a slip factor of 0.605 for a blasted specimen (Sa 2.5) with 75 μm inorganic zinc silicate. Further testing is required due to the low sample size (n = 1), however, $\mu_{EN} = 0.40$ is still supported as $\mu_{EN} = 0.44$ was obtained considering that $\mu_i \geq 0.526$ for specimens which did not slip during the test, and assuming a standard deviation of 8% of the mean.

EN 1090–2 also classifies blasted surfaces with loose rust removed as class A with $\mu_{EN} \geq 0.50$ and $\mu_{EN} = 0.50$ for design. In comparison, the present results indicated a lower value of $\mu_{EN} = 0.32$, while the previous study [4] found slip factors of $\mu_{EN} = 0.46$ and $\mu_{EN} = 0.45$, for the Sa1 and Sa3 surfaces, respectively, with due consideration of the number of samples (i.e., $n = 5$, $k_p = 2.46$, refer §3.2). In each case, however, the magnitude of the characteristic slip factor was reduced due to the relatively small number of samples, and testing of a larger sample could yield higher characteristic values. Still, only slip factors in the ranges of

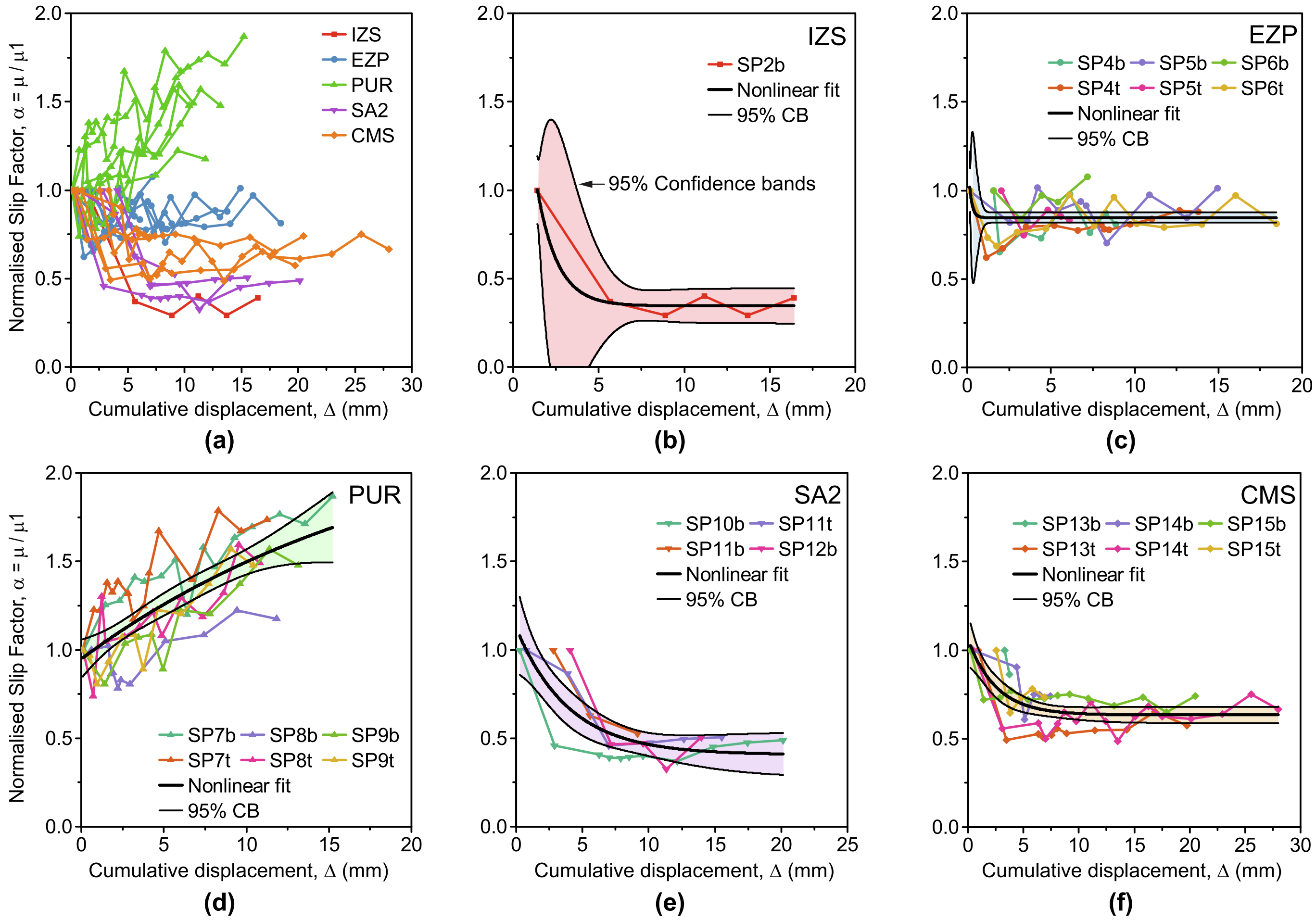

Fig. 20. Normalised slip factor ($\alpha = \mu/\mu_1$) for (a) all specimens, (b) IZS, (c) EZP, (d) PUR, (e) SA2 and (f) CMS surface finishes. Figure shows nonlinear fits using the exponential model (Eq. (11)) and 95% confidence bands (CB).

Table 6
Cyclic slip factor and cyclic initial stiffness model parameters.

	Cyclic slip factor model (Eq. (11))			Cyclic initial stiffness model (Eq. (13))		
Surface finish	a	b	c	a	b	c
IZS	2.16	0.839	0.345	0.726	0.328	0.297
EZP	0.422	5.83	0.846	0.599	0.734	0.393
PUR	−1.40	0.0497	2.35	1.04	0.225	0.0968
SA2	0.718	0.252	0.407	0.859	0.177	0.244
CMS	0.428	0.392	0.633	0.726	0.328	0.297

$0.32 \leq \mu_{EN} \leq 0.46$ and $0.39 \leq \mu_{AS} \leq 0.50$, with the latter being based on the sample minimum, can be supported by the indicated data.

Moreover, in light of the present results, consideration might be given to the reduction of the slip factor based on the potential short-term reduction (Fig. 15), which could occur if ever the connection was subjected to a cyclic action exceeding the slip resistance. For cumulative displacements nominally limited to 30 mm, the mean IZS slip factor reduced from 0.61 to 0.20, indicated as IZS: 0.61 → 0.2. Using the same notation, the other slip factor variations can be given as EZP: 0.13 → 0.10, PUR: 0.085 → 0.13, SA2: 0.45 → 0.20, and CMS: 0.20 → 0.10. As mentioned in §3.4, the slip factor generally increased for the PUR coating as the top PUR coat had a smaller slip factor than the underlying EZP layer.

4.1. Initial friction-slip model

A simplified phenomenological (i.e., fitted to experimental data) model was proposed previously as [4,29,30]

$$F(\delta) = F_s\left[1 - exp\left(\frac{-K_i\delta}{F_s}\right)\right] \tag{9}$$

where δ was the slip in the range, $0 \leq \delta \leq \delta_p$, δ_p was the effective tolerance, $F_s = \mu n_n n_s F_{p,C}$ was the slip resistance, μ was the slip factor, $F_{p,C}$ was the initial bolt tension, n_b was the number of bolts, n_s was the number of slip planes (e.g., two in the experiments), and K_i was the initial stiffness. The simplified model was fitted to the present experimental data for the first friction-slip (Fig. 18) by inputting the mean and characteristic parameters (i.e., F_s and K_i in Table 5). The exponential model provided a good fit for the force-slip behaviour of the specimens (Fig. 18), thereby supporting the applicability of the model to the behaviour of the painted specimens. Using the mean parameters (M) produced a force-slip behaviour which approximated the mean experimental behaviour, while the characteristic parameters (K) provided a reasonable lower bound. For the IZS specimens, only one value was obtained for the slip load (i.e., SP2b, §3.1), hence, the characteristic slip load could not be calculated. Consequently, Fig. 18(a) does not show the characteristic model, and only SP2b and SP2t are included for comparison with the mean model.

The model does not, however, account for the drop in force following slip, which affected the force-slip plots for all the specimens (Fig. 18). This is particularly evident for the EZP specimens (Fig. 18b). The drop in

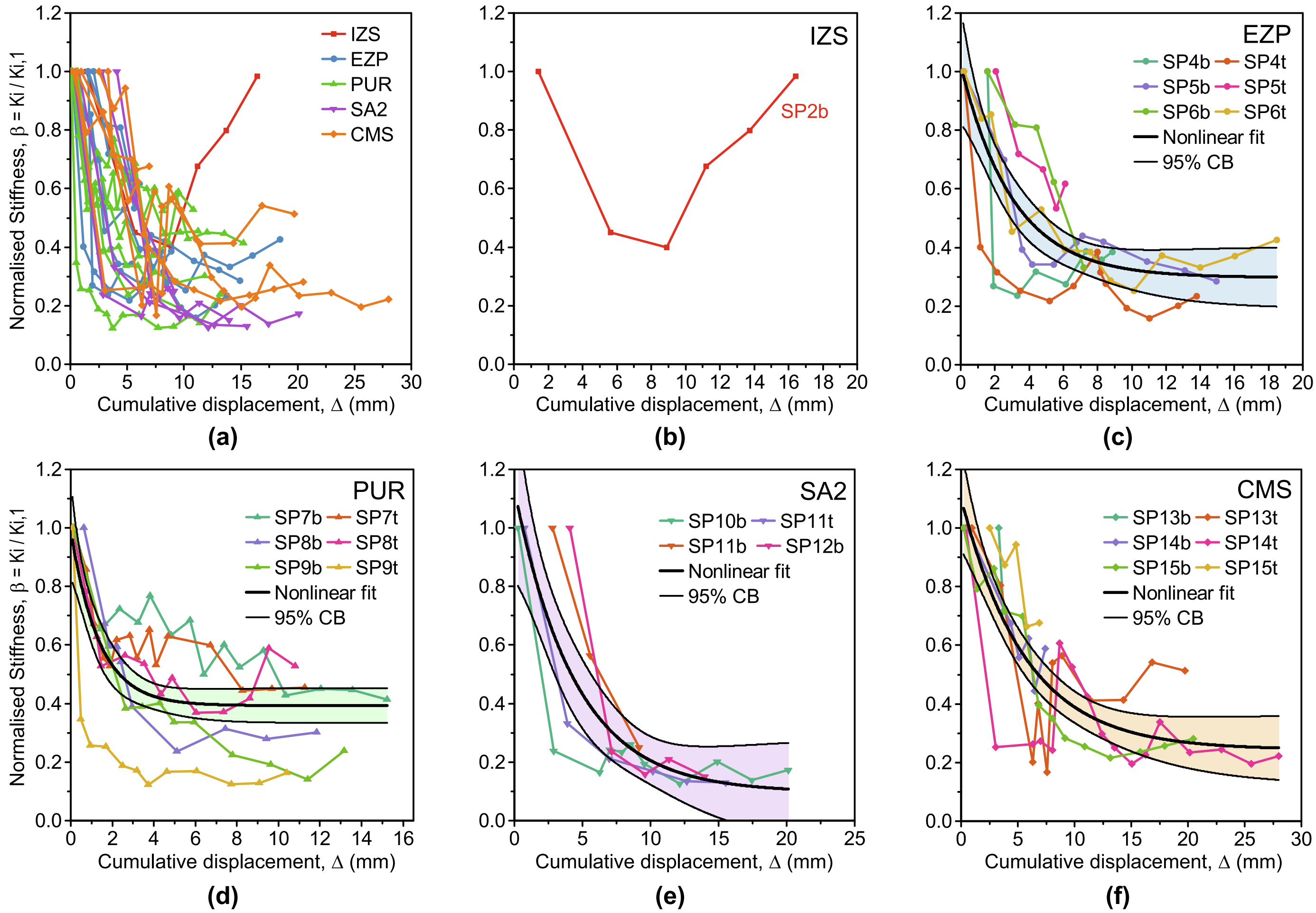

Fig. 21. Normalised initial stiffness ($\beta = K_i/K_{i,\,1}$) for (a) all specimens, (b) IZS, (c) EZP, (d) PUR, (e) SA2 and (f) CMS surface finishes. Figure shows nonlinear fits using the exponential model (Eq. (13)) and 95% confidence bands (CB).

force occurred due to the sudden release of hydraulic pressure and the transition from the static to the kinetic friction coefficient. The drop in force might be viewed as a material property since the surface finish may control the post-slip sliding velocity and, hence, the resulting dynamic friction coefficient. The influence of the test method must, however, also be acknowledged. If displacement-control was adopted, for example, then the post-slip behaviour might be different to that observed in the present test, which was force-controlled with target displacements. A drop in force may need to be considered, however, in some applications including, for example, experimental force-controlled cyclic loading or progressive collapse.

4.2. Correlation between first initial stiffness and slip factor

Correlation between the initial stiffness and the slip factor was observed for the first friction-slip cycle. For example, an approximately linear relationship can be seen by plotting the initial stiffness against the slip factor. Fig. 19a shows the linear fit with the corresponding 95% confidence bands. Average values from the previous study [4] were included for the linear fit, while the data for the IZS specimen, which had a different initial bolt preload (i.e., 63.3 kN rather than 95 kN), was excluded. Moreover, a similar correlation can be seen by plotting the initial stiffness against the related slip factor for all the friction-slip cycles of each specimen in the present study (Fig. 19b). Some deviations from the linear trend can be seen, however, as the initial stiffness does not depend solely on the related slip factor. Rather, both the initial stiffness and the slip factor are influenced to some degree by the same attributes of the sliding substrate and its surface condition.

4.3. Cyclic slip factor model

The friction-slip behaviour in the first cycle was approximated by an exponential function with two inputs. The slip load defined the maximum value of the function, while the initial stiffness controlled the initial curvilinear behaviour. The force-slip behaviour in subsequent load cycles can be approximated by the same exponential function, provided that the slip load and initial stiffness are adjusted accordingly. Alternatively, other hysteretic models can be derived based on the following parameter variations.

The slip load can be calculated based on the initial bolt tension and the corresponding slip factor (Eq. (4)). The slip factor can be given as

$$\mu = \alpha\mu_1 \tag{10}$$

where μ_1 is the first slip factor and α is a factor accounting for the variation of the slip factor with the cumulative displacement. An exponential plateau model can be applied and α can be given as

$$\alpha = \frac{\mu}{\mu_1} = a\exp(-b\Delta) + c \tag{11}$$

where a, b, and c are parameters.

The initial value, $\alpha(\Delta = 0)$, is equal to $a + c$, and generally has a value close to 1. The plateau is equal to c, which reflects the ratio between the first slip factor and the slip factor for a large cumulative displacement (i.e., $\Delta \rightarrow 30$ mm). The parameters a and b control the rate of change with respect to the cumulative displacement (i.e., $\alpha'(\Delta = 0) = ab$). For the IZS, EZP, SA2 and CMS specimens, an exponential decay model is appropriate, hence, $a > 0$ and $0 < c < 1$. For the PUR specimens, an exponential growth model is appropriate, hence, $a < 0$ and $c > 1$.

The exponential equation (Eq. (11)) was fitted to the data for the IZS, EZP, PUR, SA2, and CMS specimens (Fig. 20). The resulting parameters (Table 6) may be used to estimate the nominal variation of the slip factor with the increasing cumulative displacement.

4.4. Cyclic initial stiffness model

The initial stiffness can similarly be given as

$$K_i = \beta K_{i,1} \tag{12}$$

where $K_{i,1}$ is the first initial stiffness and β is a factor accounting for the variation of the stiffness with the cumulative displacement. The present results generally showed that the stiffness reduced with the increasing cumulative displacement (Δ), hence, β can be given as

$$\beta = \frac{K_i}{K_{i,1}} = aexp(-b\Delta) + c \tag{13}$$

where a, b, and c are parameters. The initial value, $\beta(\Delta = 0)$, is equal to $a + c$ and depends on the cumulative displacement at the first slip. The lower limit is equal to c which reflects the ratio between the first stiffness and the stiffness after a large cumulative displacement (i.e., $\Delta \to 30$ mm), and parameters a and b control the rate of change with respect to cumulative displacement (i.e., $\beta'(\Delta = 0) = ab$).

The exponential equation (Eq. (13)) was fitted to the data for the EZP, PUR, SA2, and CMS specimens (Fig. 21). The resulting parameters (Table 6) may be used to estimate the nominal reduction of the initial stiffness with the increasing cumulative displacement.

5. Conclusions

The short-term cyclic friction-slip behaviour of the AS/NZS 3678–350 steel (G350) material was investigated by conducting experiments on bolted steel connections consisting of EN 1090–2 slip factor test assemblies with M16 bolts. Five commonly used surface finishes were considered including inorganic zinc silicate (IZS), epoxy zinc primer (EZP), aliphatic acrylic polyurethane (PUR), abrasive blasted (SA2), and clean mill scale (CMS). The main findings are summarised as follows.

1. The first slip factors and initial stiffness were determined for each specimen. The mean and characteristic values were derived for each surface finish (Table 3 & Table 4).
2. Based on the present results, the AS 4100:2020 first slip factor $\mu_{AS} = 0.35$ for clean "as-rolled" surfaces could be too high in some cases. A lesser value of 0.20 is suggested for general design in the absence of more specific test results. This finding is consistent with EN 1090–2:2018, which also specifies a first slip factor of 0.20 for surfaces as rolled.
3. A simplified model was fitted to the experimental data for the first force-slip behaviour by inputting the mean and characteristic parameters (i.e., first slip factor and initial stiffness). The exponential model provided a good fit and demonstrated the applicability of the model to the uncoated and coated steel materials.
4. Correlation between the first initial stiffness and the slip factor was observed as an approximately linear relationship. However, some deviations from the linear trend were noted as the first initial stiffness does not depend solely on the related slip factor.
5. The effects of the cyclic loading on the slip factor and initial stiffness were evaluated and discussed. The variation of each was related to the cumulative displacement as a measure of the progressive degradation of the faying surfaces. For each surface condition, simplified models were fitted to the experimental data to estimate the cyclic slip factor and initial stiffness for design purposes.

CRediT authorship contribution statement

Andrew William Lacey: Conceptualization, Methodology, Investigation, Formal analysis, Visualization, Writing – original draft. **Wensu Chen:** Funding acquisition, Supervision, Validation, Writing – review & editing. **Hong Hao:** Supervision, Validation, Writing – review & editing.

Declaration of Competing Interest

The authors declare that they have no known competing financial interests or personal relationships that could have appeared to influence the work reported in this paper.

Data availability

Data will be made available on request.

Acknowledgements

The authors acknowledge the financial support from the Australian Government through the Australian Research Council (ARC) Future Fellowship (FT210100050). The authors also acknowledge the contribution of Yii Xian Tien through the related undergraduate Civil Engineering Research Project.

References

[1] A.W. Lacey, W. Chen, H. Hao, K. Bi, Structural response of modular buildings - an overview, J. Build. Eng. 16 (2018) 45–56, https://doi.org/10.1016/j.jobe.2017.12.008.
[2] D.J.L. Kennedy, High strength bolted galvanized joints, J. Struct. Div. Proc. Am. Soc. Civ. Eng. 98 (1972) 2723–2738, https://doi.org/10.1061/JSDEAG.0003399.
[3] A.W. Lacey, W. Chen, H. Hao, K. Bi, Effect of inter-module connection stiffness on structural response of a modular steel building subjected to wind and earthquake load, Eng. Struct. 213 (2020), 110628, https://doi.org/10.1016/j.engstruct.2020.110628.
[4] A.W. Lacey, W. Chen, H. Hao, K. Bi, Experimental and numerical study of the slip factor for G350-steel bolted connections, J. Constr. Steel Res. 158 (2019) 576–590, https://doi.org/10.1016/j.jcsr.2019.04.012.
[5] Standards Australia, AS/NZS 3678 Structural Steel - Hot Rolled Plates, Floorplates and Slabs, Standards Australia, Sydney, Australia, 2016.
[6] CEN, EN 1090–2:2018 Execution of Steel Structures and Aluminium Structures - Part 2: Technical Requirements for Steel Structures, European Committee for Standardization (CEN), Brussels, Belgium, 2018.
[7] Standards Australia, AS 1627.4–2005 (R2017) Metal Finishing - Preparation and Pretreatment of Surfaces, Part 4: Abrasive Blast Cleaning of Steel, Standards Australia Limited, Sydney, Australia, 2005.
[8] SIS, The Rust Grade Book, ISO 8501-1: Preparation of Steel Substrates before Application of Paints and Related Products — Visual Assessment of Surface Cleanliness — Part 1: Rust Grades and Preparation Grades of Uncoated Steel Substrates and of Steel Substrates after Overall Removal of Previous Coatings, Swedish Standards Institute (SIS), Switzerland, 2007.
[9] S. Vitelleschi, L.C. Schmidt, Influence of Cyclic Loading on the Slip Factor for Friction-Grip Joints CE 2, Inst Eng Aust Civ Eng Trans, 1978, pp. 112–119.
[10] W.Y. Loo, P. Quenneville, N. Chouw, The influence of surface preparation and the lubricating effect of mill scale on the performance of slip-friction connectors, Constr. Build. Mater. 155 (2017) 1025–1038, https://doi.org/10.1016/j.conbuildmat.2017.08.100.
[11] W.Y. Loo, P. Quenneville, N. Chouw, A new type of symmetric slip-friction connector, J. Constr. Steel Res. 94 (2014) 11–22, https://doi.org/10.1016/j.jcsr.2013.11.005.
[12] C.E. Grigorian, T.S. Yang, E.P. Popov, Slotted bolted connection energy Dissipators, Earthquake Spectra 9 (1993) 491–504, https://doi.org/10.1193/1.1585726.
[13] Y.-B. Wang, Y.-Z. Wang, K. Chen, G.-Q. Li, Slip factors of high strength steels with shot blasted surface, J. Constr. Steel Res. 157 (2019) 10–18, https://doi.org/10.1016/j.jcsr.2019.01.023.
[14] CEN, EN 14399–3:2005 High-strength Structural Bolting Assemblies for Preloading - Part 3: System HR - Hexagon Bolt and Nut Assemblies, in: European Committee for Standardization, 2005.
[15] Standards Australia, AS/NZS 1252.1:2016 High-strength Steel Fastener Assemblies for Structural Engineering - Bolts, Nuts and Washers, Part 1: Technical Requirements, Standards Australia Limited, Sydney, Australia, 2016.

[16] CEN, EN 14399–2:2015 High-strength Structural Bolting Assemblies for Preloading - Part 2: Suitability for Preloading, European Committee for Standardization (CEN), Brussels, Belgium, 2015.
[17] Standards Australia, AS 3894.5 Site Testing of Protective Coatings, Method 5: Determination of Surface Profile, Standards Australia Limited, Sydney, Australia, 2002.
[18] Standards Australia, AS 2312.1 Guide to the Protection of Structural Steel against Atmospheric Corrosion by the Use of Protective Coatings, Part 1: Paint Coatings, SAI Global Limited, Sydney, Australia, 2014.
[19] G.F. Cavallaro, A.B. Francavilla, M. Latour, V. Piluso, G. Rizzano, Cyclic response of low yielding connections using different friction materials, Soil Dyn. Earthq. Eng. 114 (2018) 404–423, https://doi.org/10.1016/j.soildyn.2018.07.041.
[20] H.-H. Khoo, C. Clifton, J. Butterworth, G. MacRae, G. Ferguson, Influence of steel shim hardness on the sliding hinge joint performance, J. Constr. Steel Res. 72 (2012) 119–129, https://doi.org/10.1016/j.jcsr.2011.11.009.
[21] E.P. Popov, C.E. Grigorian, T.-S. Yang, Developments in seismic structural analysis and design, Eng. Struct. 17 (1995) 187–197, https://doi.org/10.1016/0141-0296(94)00006-F.
[22] R.E. Walpole, R.H. Myers, S.L. Myers, K. Ye, Probability & Statistics for Engineers & Scientists, 9th ed., Pearson Education Limited, Harlow, Essex, England, 2016.
[23] M. Holický, Introduction to Probability and Statistics for Engineers, Springer, London, 2013.
[24] Standards Australia, AS 4100:2020 Steel Structures, Standards Australia Limited, 2020.
[25] G.L. Kulak, J.W. Fisher, J.H.A. Struik, Guide to Design Criteria for Bolted and Riveted Joints, 2nd ed., American Institute of Steel Construction, Inc., Chicago, IL, USA, 2001.
[26] A. Cruz, R. Simões, R. Alves, Slip factor in slip resistant joints with high strength steel, J. Constr. Steel Res. 70 (2012) 280–288, https://doi.org/10.1016/j.jcsr.2011.11.001.
[27] Y. Tamba, S. Yukito, S. Kimura, T. Yamaguchi, K. Sugiura, Slip coefficient for high-strength bolted frictional joints with roughened steel surface and inorganic zinc-rich painted surface, J. JSCE. 3 (2015) 19–32, https://doi.org/10.2208/journalofjsce.3.1_19.
[28] Y.-B. Wang, Y.-Z. Wang, K. Chen, H.-J. Jin, Slip factor of high strength steel with inorganic zinc-rich coating, Thin-Walled Struct. 148 (2020), 106595, https://doi.org/10.1016/j.tws.2019.106595.
[29] A.W. Lacey, W. Chen, H. Hao, K. Bi, New interlocking inter-module connection for modular steel buildings: simplified structural behaviours, Eng. Struct. 227 (2021), 111409, https://doi.org/10.1016/j.engstruct.2020.111409.
[30] A.W. Lacey, W. Chen, H. Hao, K. Bi, Lateral behaviour of modular steel building with simplified models of new inter-module connections, Eng. Struct. 236 (2021), 112103, https://doi.org/10.1016/j.engstruct.2021.112103.